COMPUTATIONAL ANALYSIS OF AcDS IN CA1 AND CA3 PYRAMIDAL NEURONS WITH AXON CARRYING DENDRITES

by

Gül ÖNCÜ

BSc, in Chemistry, Boğaziçi University, 2013

Submitted to the Institute of Biomedical Engineering
in partial fulfillment of the requirements
for the degree of
Master of Science
in
Biomedical Engineering

Boğaziçi University
2018

COMPUTATIONAL ANALYSIS OF AcDS IN CA1 AND CA3 PYRAMIDAL NEURONS WITH AXON CARRYING DENDRITES

APPROVED BY:

Prof. Dr. Hale Saybaşılı (Thesis Advisor)	.....
Assist. Prof. Dr. Pınar Öz (Thesis Co-advisor)	.....
Prof. Dr. Burak Güçlü	.....
Assist. Prof. Dr. Esin Öztürk Işık	.....
Assist. Prof. Dr. Mehmet Kocatürk	.....

DATE OF APPROVAL: 11 June 2018

ACKNOWLEDGMENTS

I would like to thank to Prof. Dr. Hale Saybaşılı for opening her lab to me, her support and help in every aspect.

I also would like to thank to Assist. Dr. Pınar Öz for being the connection between science and me, for believing in me, for encouraging me to do what I like the most and for staying with me until midnight just because I was working. Without her, I would not be able to either finish my thesis or apply to PhD. She is beyond an advisor for me for changing my life that I cannot express my gratitude.

Finally, to Özgür Can, Derya Karagöz, Sevda Öncü and Yavuz Öncü for showing an incredible support during my masters degree. Without their psychological support, I would not be able to handle this process.

ACADEMIC ETHICS AND INTEGRITY STATEMENT

I, Gül Öncü, hereby certify that I am aware of the Academic Ethics and Integrity Policy issued by the Council of Higher Education (YÖK) and I fully acknowledge all the consequences due to its violation by plagiarism or any other way.

Name :

Signature:

Date:

ABSTRACT

COMPUTATIONAL ANALYSIS OF AcDS IN CA1 AND CA3 PYRAMIDAL NEURONS WITH AXON CARRYING DENDRITES

Pyramidal neurons are the most abundant excitatory cell type in cortex and hippocampus. The canonical topology of these glutamatergic neurons consists of a pyramidal-shaped soma, an apical dendrite extending vertically between layers, basal dendrites extending horizontally in the same layer and an axon extending from soma.

However, the recent studies show that some hippocampal pyramidal neurons on Cornu Ammonis (CA) of healthy mammalian brain possess an axon that is placed on the basal dendrite in many instances. This phenomenon is observed in 50% in CA1 and 30% in CA3 and in these cell types the stimulus is privileged on the AcD. The effect on information processes is thought to be in hippocampal trisynaptic circuits are not clarified yet. Neither the reason behind this differentiation nor the circumstances under which this phenomenon occurs is discovered. In this study, CA1 and CA3 pyramidal neurons with AcDs and with regular neurites are modeled on NEURON simulation platform for understanding the function of axon-carrying dendrites.

The results showed a significant difference in the potential conservation in AcD cells compared to nonAcD cells and privilege on the AcD branches which can enhance the plasticity and LTP processes.

Keywords: AcDs, Pyramidal Neurons, Hippocampus, CA1, CA3.

ÖZET

AKSON TAŞIYAN DENDRİTLİ CA1 VE CA3 PİRAMİDAL NÖRONLARININ HESAPLAMALI ANALİZİ

Piramidal nöronlar korteks ve hipokampus sinir ağlarında en fazla bulunan uyarıcı hücre tipidir. Bu glutamaterjik nöronların temel morfolojisi, piramit biçimli bir hücre gövdesi, dendritik dikenlere sahip katmanlar arası uzanan apikal dendrit, hücre gövdesinin bulunduğu katmanda bağlantı kuran bazal dendritler ve hücre gövdesinden çıkan akson şeklindedir.

Ancak, son yıllarda yapılan çalışmalar, sağlıklı memeli beyninde Cornu Ammonis (CA) üzerinde yer alan piramidal nöronların önemli bir kısmında aksonun bir bazal dendrit üzerinde taşındığını (AtD) göstermiştir. CA1'de yaklaşık %50 ve CA3'te yaklaşık %30 oranlarında görülebilen bu tip hücrelerde AtD'ye gelen uyaranlara ayrıcalık verildiği düşünülmektedir. Bu hücrelerin hipokampal trisinaptik devredeki bilgi işleme süreçlerine etkisi ise henüz tam olarak aydınlatılmamıştır. Hücrelerin ne amaçla bu yönelimi gösterdiği ve hangi hücrelerin yapısının farklılaşacağının seçildiğibilinmemektedir. Bu yapının oluşma sebeplerinin bulunması amacıyla çalışmamızda geleneksel fizyolojiye sahip CA1 ve CA3 piramidal nöronları ile AtD'ye sahip CA1 ve CA3 piramidal sinir hücreleri NEURON simülasyon platformunda modellenmiştir.

Sonuçlar AtD'ye sahip hücrelerde klasik nöronlara kıyasla potansiyelin önemli ölçüde korunduğunu ve AtD'ye öncelik verildiğini göstermiştir. Bu sebeple AtD yapısının plastisite ve LTP süreçlerinin iyileştirilmesinde katkısı olduğu düşünülmektedir.

Anahtar Sözcükler: Akson taşıyan dendritler, piramidal nöronlar, hipokampus, CA1, CA3.

TABLE OF CONTENTS

LIST OF FIGURES

LIST OF TABLES

LIST OF ABBREVIATIONS

DG	Dentate Gyrus
CA	Cornu Ammonis
CA1	Cornu Ammonis Area 1
CA2	Cornu Ammonis Area 2
CA3	Cornu Ammonis Area 3
CA4	Cornu Ammonis Area 4
EC	Entorhinal Cortex
MEA	Medial Entorhinal Cortex
Sub	Subiculum
PrS	Presubiculum
PaS	Parasubiculum
POR	Postrhinal Cortex
EPSP	Excitatory Postsynaptic Potential
IPSP	Inhibitory Postsynaptic Potential
ADP	Spike afterdepolarization
L	Section Length
Diam	Diameter
Lm	Lamina Moleculare
AIS	Axon Initial Segment
NR	Node of Ranvier
Ra	Cytoplasmic Resistivity
Cm	Specific Membrane Capacitance
AcD	Axon Carrying Dendrites
non-Acd	Regular dendrites
El	Leakage Reversal Potential
AP	AP

1. INTRODUCTION

1.1 Hippocampus

Hippocampus is a sea-horse shaped formation placed in the limbic system. Being a part of the forebrain, it is in the medial temporal lobe [9]. It works as the search engine of the brain, transfers the newly acquired memories to neo-cortex and calling them back when needed, thus it is effective in cognitive functions along with emotional and other sensory components [10, 11]. It also has a role in spatial orientation [12, 13]. The same formation is observed across all ranges of mammals and some primitives as well, thus its constitution is evolutionally conserved [14].

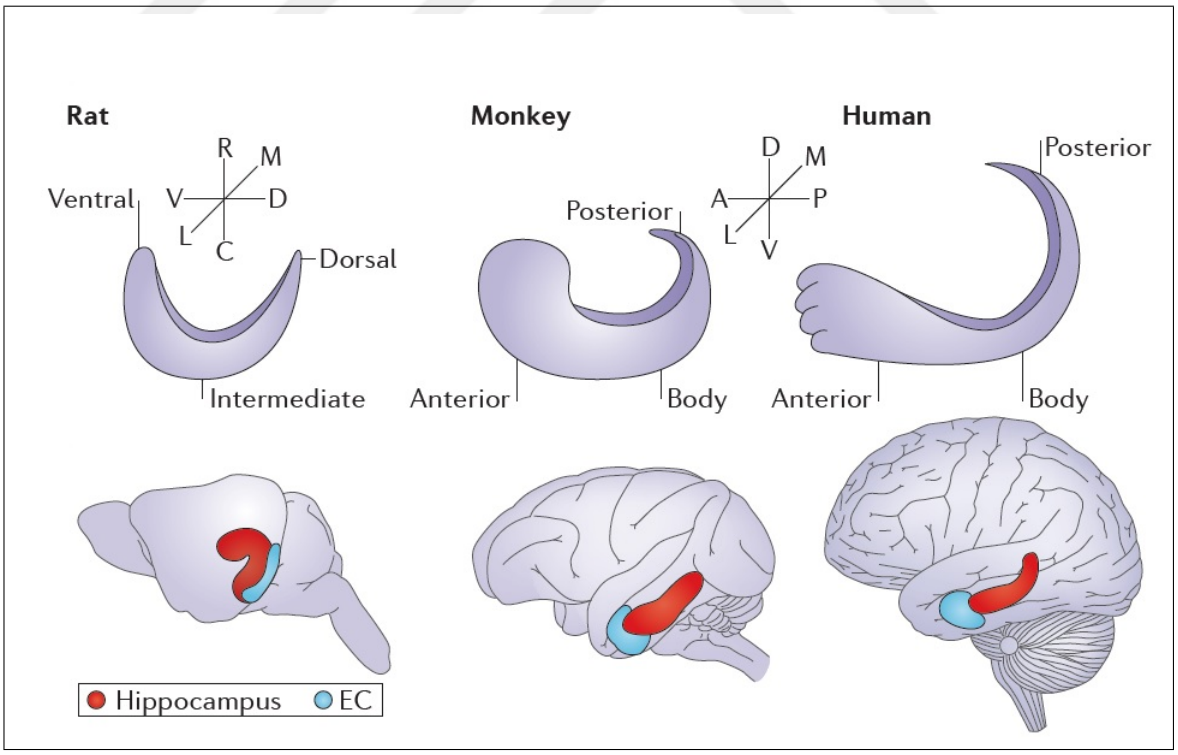

Figure 1.1 The full long axis of the hippocampus (red) can be seen in brains of rats, macaque monkeys and humans, with the entorhinal cortex (EC) shown in blue [1].

In studies of rodent hippocampus, multi-neuron recordings show that single CA1 neurons increased their AP firing rate whenever it passes a certain place or an environment [11]. This study was important for showing the nature of information processing in hippocampal networks as well as the role of hippocampus on spatial recognition. However, each hippocampal subgroup receives different combinations of projections from entorhinal cortex [15]. This implies that each subgroup has a different role in information processing and in integrating the received information.

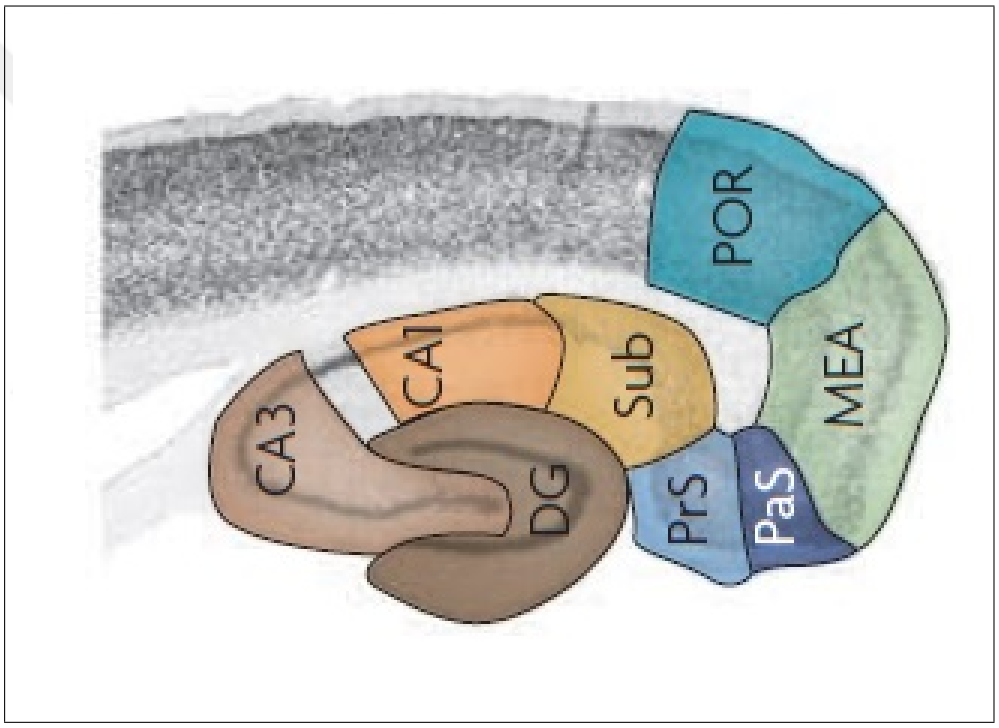

Figure 1.2 Hippocampal and parahippocampal subregions with color codes [2].

Hippocampus is composed of 2 separate layers; *Dentate Gyrus* (DG) capping *Cornu Ammonis* (CA). The structure is observable without staining due to fine orientation of the grey matter. CA is further categorized into 4 subgroups based on their cellular morphology and synaptic inputs detected with Golgi impregnation [16]: CA1, CA2, CA3 and CA4 as shown in Figure 1.2 . Each CA subfield has its own functional characteristics with the uniqueness of each area being particularly prominent in the way information is represented at the neural ensemble level [17, 18]. CA2 is generally

considered as a transition state due to its small size. The subgroups of hippocampus differ by size, shape, electrophysiological properties, connectivity and morphology [11].

1.1.1 Trisynaptic Loop

The CA subfields are connected by excitatory connections through the trisynaptic pathway for transmission of information in the hippocampus [19]. The term refers to the circuitry between *Entorhinal Cortex* (EC), DG, CA3 and CA1. The description of the trisynaptic circuit led to the idea that the CA subfields, especially the CA1 and CA3 regions, correspond to successive processing stages in a major feed-forward loop through the hippocampus [20].

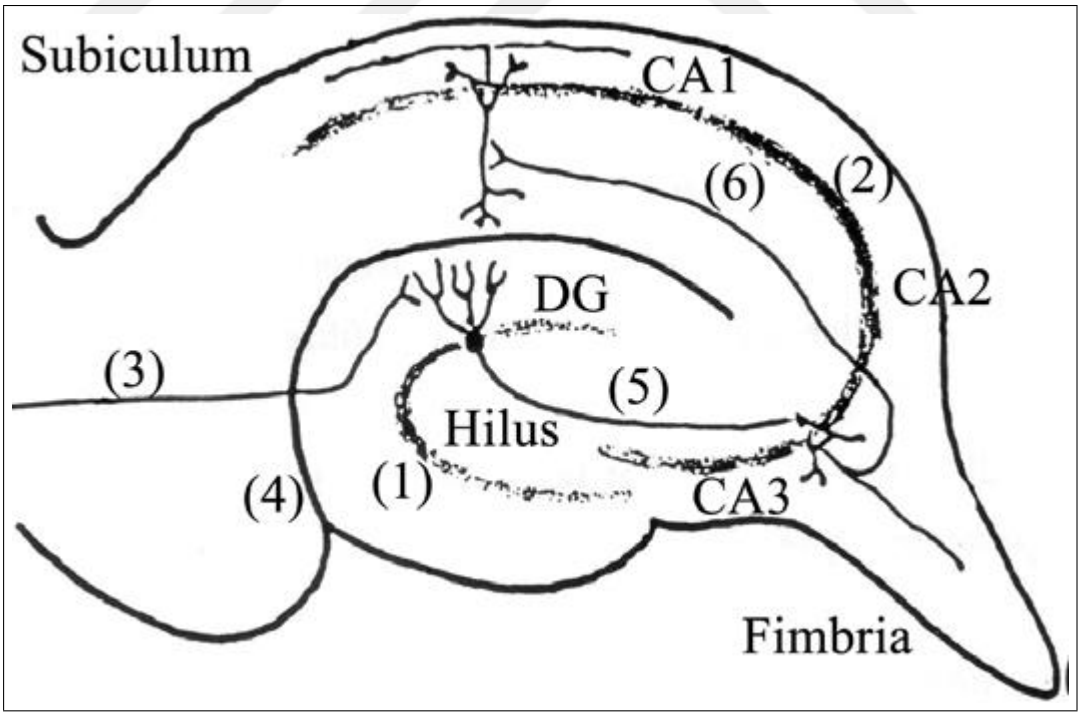

Figure 1.3 Schematic expression of hippocampal subfields and trisynaptic loop [3].

Within the first link, the input is transferred from layer II EC. Axons of pyra-

midal cells (perforant fibers) pass through *stratum moleculare* of DG, which mediate rapid pattern separation in the hippocampal network [21] and then projected on the granule cells. After that, the input is transferred from the axons of the granule cells to pyramidal cells of CA3. The second link is between the Schaeffer collaterals of CA3 towards CA1 pyramidal cells. The third link is developed from CA1 to *Entorrhinal Cortex*, completing the loop. Apart from this major network within hippocampus, hippocampal interneurons, basket cells, mossy cells and granule cells are also incorporated in the feedback mechanism [22].

1.1.2 Pyramidal Neurons

Pyramidal neurons, named due to their pyramid-like soma shape, is the most abundant principal neuron type in the mammalian cerebral cortex [4] and can be found in various regions of the central nervous system, especially in the forebrain structures in mammals such as cerebral cortex, amygdala and hippocampus. However, the olfactory bulb, the striatum, the midbrain, the hindbrain or the spinal cord do not contain pyramidal neurons [23]. Its location suggests the pyramidal neurons to have an essential role in cognitive functions. Pyramidal neurons can be observed in primitive animals like fish or rodents, so it is an evolutionally conserved structure.

Like other neurons, pyramidal cells have a single axon to produce and transmit the output and multiple dendrites to receive inputs, however they are both branched excessively. Unlike other neuron cells, pyramidal cells can transfer the information bidirectional [24]; meaning they can receive information from axon and give output via dendritic branches. Its highly branched structure enables the neuron to transfer information between both the neighboring pyramidal cells and the cells in different layers. Yet, pyramidal cells can possess different structures among the sections they exist.

Another feature that distinguishes pyramidal cells from each other is how they

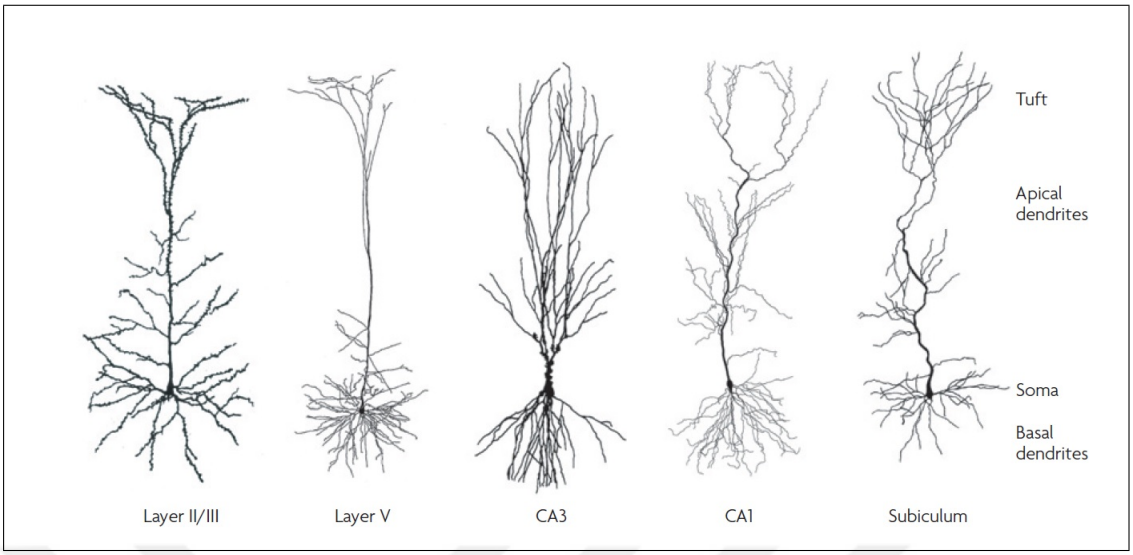

Figure 1.4 Pyramidal neurons in layer II/III, layer V, CA3, CA1 and subiculum [4].

respond to current injection. Even though the response strongly depends on the stimulus itself, most of the pyramidal cells show a characteristic response by giving a continuous train of spikes to the stimulus. Highly branched architecture of the pyramidal neurons plays a crucial role in this characteristic behavior as well as the unique characteristic of their ion channels that generate the AP.

These pyramidal neurons differ from each other by their size, dendritic branching or electrophysiological properties, yet they can still be identified by their elongated apical dendrite containing a tuft of dendrites and relatively short basal dendritic branching which enables the pyramidal cells to communicate with the neurons in the same layer as well as the other layers. Figure 1.4 shows the pyramidal neurons in different cortical layers or in hippocampus have distinctive features as well as their similarities.

Morphologies of apical dendrites and basal dendrites suggest that the information received from other neurons can be integrated differently depending on the location the information is received. Different dendritic domains receive information from different brain locations. For example, as mentioned in section 1.1.1 Trisynaptic Loop, CA1 neurons receive input from EC through distal tuft, whereas the remaining dendrites receive information from CA3 through Schaffer collaterals [25]. In regard, inputs from different domains may be integrated differently.

As humans have the most complex, branched and spine-rich dendrites in pyramidal cells compared to other primates [26] and the pyramidal cells are the most abundant cell type found in the prefrontal cortex, it is thought to be paralleled with the cognitive and functional capacity.

In this study, hippocampal CA1 and CA3 pyramidal neurons are studied and modeled due to their newly discovered distinctive properties.

1.1.3 CA1 Region

CA1 region is the primary output region of hippocampal network and major distal output target of CA3 pyramidal neurons. Most of the output projects to entorhinal cortex, the second pathway is to subiculum. The main cell type of CA1 is pyramidal neurons, with somata aligned on *stratum pyramidale* [27].

The CA1 region of the rat hippocampus is larger than other CA regions; In rats, CA1 spans 3.2 mm x 3.5 mm of the anteroposterior and mediolateral plane and almost 6.0 mm of the dorsoventral axis. Based on the difference of connection to extrahippocampal regions, CA1 is further divided into CA1a, CA1b and CA1c along the transverse axis. CA1 differs from other hippocampal regions for its apoptotic mechanisms.

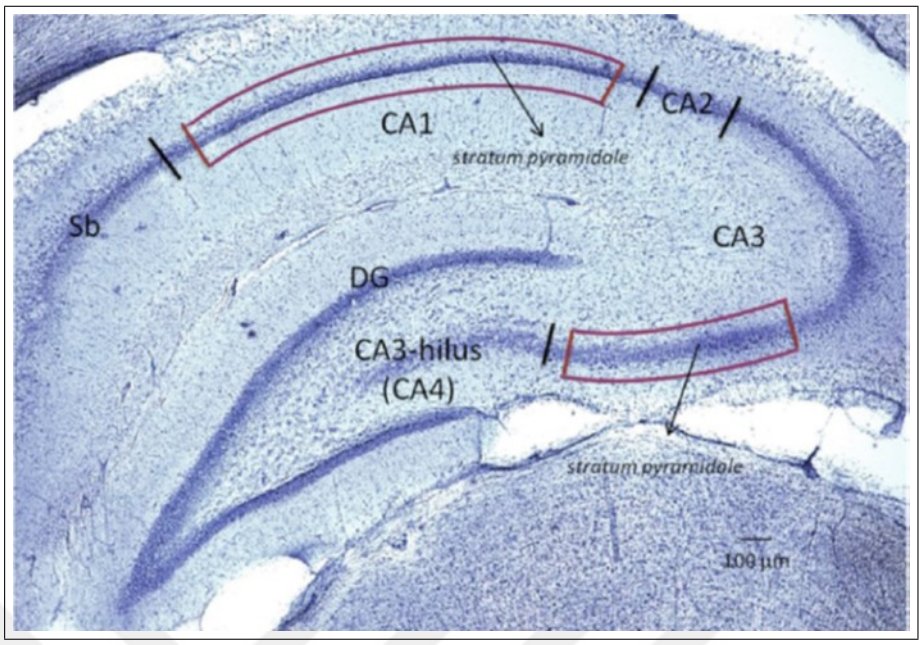

Figure 1.5 Hippocampal morphology and subregions [5].

Since episodic memory formation and learning are very complex mechanisms, the subregions are thought to have different roles in this process. CA1 pyramidal neurons are found to have a role in recognizing the novelty of an event or a context and acquisition of spatial memory [28], whereas non-spatial memory is not affected by the lesion [29, 30].

Another synaptic loop that involves CA1 is called monosynaptic loop in which the information is transmitted from EC to CA1 and then sent back to EC again. This short loop is found to be necessary for incremental spatial learning [31].

1.1.4 CA3 Region

Another important element of the hippocampal network is the CA3 pyramidal neuron cluster. The information is received from dentate gyrus to CA3 pyramidal cells and from here it is primarily sent to CA1 pyramidal cells. Proximal CA3 projections are connected to CA1 pyramidal neurons septal to their location and distal CA3 neurons

project to temporal CA1 pyramidal neurons [32].

The synapses of CA3 pyramidal cells are not homogeneous and they are modifiable [33]. In addition to that a significant number of synapses are silenced postsynaptically during pairing induced LTP in the hippocampus [34]. This functional silencing with inhomogeneous and modifiable synapses show that the functional connectivity may be different than structural connectivity.

CA3 pyramidal cells are required in the rapid one-trial contextual learning, memory acquisition of one-time experience, associative memory recall, for pattern completion-based memory recall, and for spatial tuning of CA1 cells [31]-[35].

1.2 Neural Processing

To transmit signals for long distances in our body without loss or weakening, the neurons need to amplify the signals continuously. When a depolarizing potential propagates, Na^+ open in response. The core responsibility in this process belongs to voltage gated Na^+ channels.

The Na^+ ions outside the membrane passes through this channel and flow into the cell, further depolarizing the membrane. Within a very short time the equilibrium is reached, and channels are repositioned to inactivated state. In this position, the cell can recover its former electrical potential at the resting state and becomes ready for another stimulation. Then, the Na^+ channels become closed again as its first position.

When no stimulus is present, Na^+ channels remain closed and the membrane potential is constant at about -80 mV. However, when a stimulus is applied the potential depolarizes and allows the Na^+ ions inside, permitting Na^+ ions to enter the axon along their concentration gradient. If the depolarization is sufficient, even more Na^+ channels are open and the membrane potential rapidly approaches the equilibrium potential for Na^+ about +40 mV. At this point the Na^+ channels close adopting the

inactive conformation. The channel is unable to open again even though the membrane potential is still depolarized. The Na^+ channels remain in this inactivated state until a few milliseconds after, the membrane potential returns to its initial negative value. The AP is propagated along the length of the axon in only one direction. By examining the membrane potential, and state of the Na^+ channels along the length of the axon, we understand the reason.

As a depolarizing stimulus reaching our section of the membrane, Na^+ channels open and current flows into the axon. This in turn depolarizes adjacent sections of the membrane causing adjacent Na^+ channels to open. And the AP is thus propagated along the axon. Na^+ channel inactivation prevents the depolarization from spreading backward along the axon.

AP initiation starts in the where both IPSP and EPSP are summed before the information is transmitted to the axon. As in many other neurons, APs are usually generated at the AIS [36] since this region has the lowest voltage threshold for spike generation [37, 38]. Since the potential initiation starts in this segment, its nature (i.e. number of ion channels) is strongly decisive in the AP characteristic.

Classical neurons are composed of a soma, dendrites and an axon connected to soma separately. Dendritic branches receive the input from the other cells and the media, transmits the inputs to soma. Soma sums up the EPSPs and IPSPs received from the dendritic trees and transmits the output via axon which is connected to the soma with axon hillock. The AP is generated in the which is highly plastic and can change its length and its position along the axon in a homeostatic manner.

Synapses distant to soma has lower impact compared to synapses that are closer to soma. The reason is the electrical attenuation during the transmission of the current flow [39]. To compensate this attenuation phenomena, distal synapses have tendency to have smaller diameters as smaller diameters have higher input impedance. They also have higher number of neurotransmitter receptors on the distal ends and the inputs are integrated. Developing different mechanisms to increase synaptic efficiency

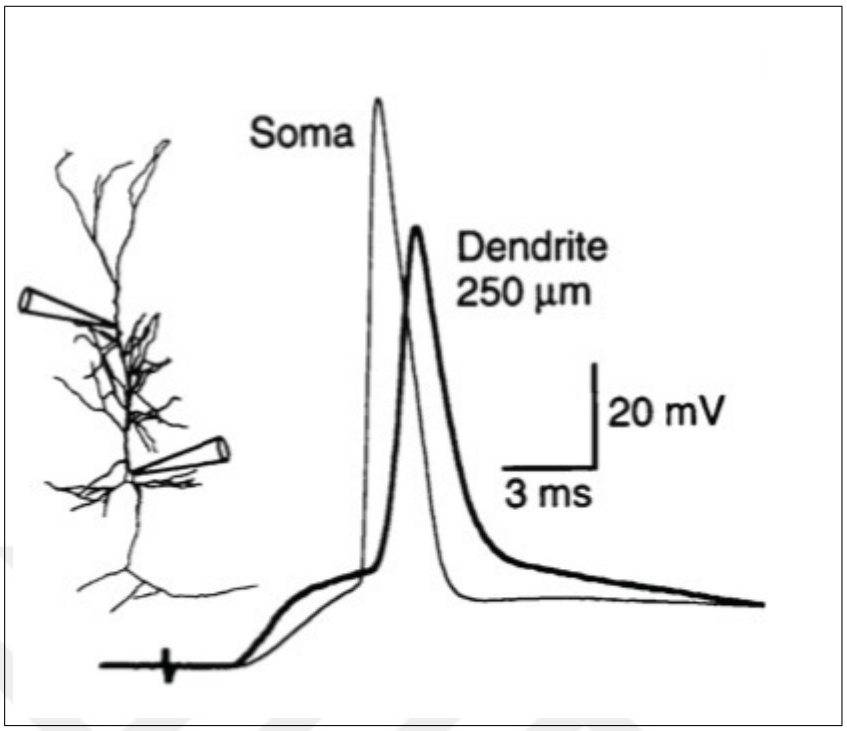

Figure 1.6 APs simultaneously recorded from soma and apical dendrite of a CA1 pyramidal neuron [6].

is common in hippocampal CA1 and CA3 pyramidal neurons. However, this biological normalization is not observed in all of the neurons due to its biological inefficiency [40].

AP characteristics also depend on many factors and they are different in every cell type. Voltage gated channels have impact on AP threshold, spike afterhyperpolarization (AHP), spike afterdepolarization (ADP) and AP firing mode. Some pyramidal neurons respond to somatic current injections with regular spikes with frequency adaptation, however some pyramidal neurons show intrinsic firing patterns. This also depends on AP waveform. APs in pyramidal neurons are generally followed by ADP and the size of the ADP impacts the neuron to either regularly spike or intrinsically fire [41]. Furthermore, the neuronal response is affected by dendritic channels and dendritic structures.

1.2.1 Spike Trains

When an electrode is placed near soma or axon of a neuron, the short pulses of APs can be measured. These short pulses are called "spikes". A typical spike has 1-2 ms duration and 100 mV amplitude. Figure 1.7 shows an example of spike trains collected from different regions of a CA1 pyramidal neuron. Neurons typically communicate with a series of APs called "spike trains" rather than a single AP. The form of AP is more or less similar in neurons and the form is not important in information transfer, the main element is the number and timing of spikes. AP is the base unit of these spikes.

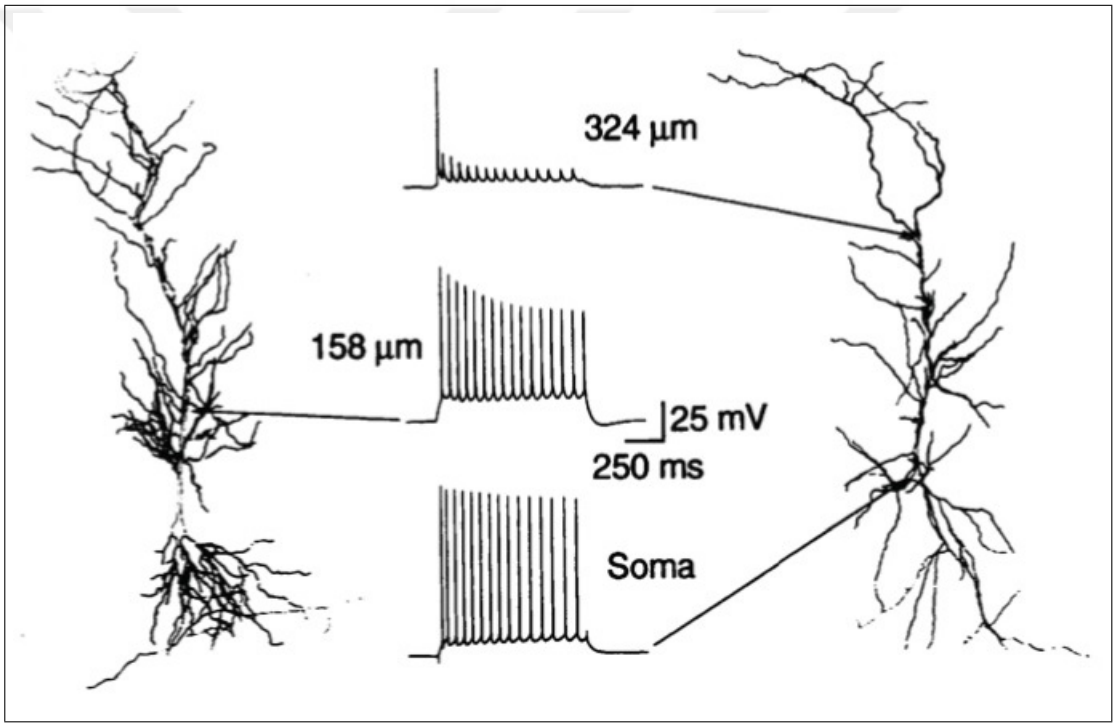

Figure 1.7 Spike trains recorded from soma and dendrites after current injection to soma in CA1 pyramidal neurons [6].

APs require time to fire another one. This provides spikes to be well separated as in bar codes. The minimum time required for a neuron to fire another AP is called "refractory period". Refractory period determines the minimum space between the spikes. It is not possible to fire before the certain refractory period of a neuron regardless of the input's strength. Absolute refractory period is followed by a relative refractory period, in which it is very hard - but not impossible- to excite a neuron. The postsynaptic neuron receives several spikes from presynaptic neurons. If the num-

ber of spikes exceed a certain threshold, then the AP generation is triggered in the postsynaptic neuron, which in turn is sent from axon as the output.

The spike trains are examined in 3 different ways in general; 1) average number of spikes over time, 2) average number of spikes over several repetitions of the experiment, 3)average number of spikes over a population of neurons.

1.3 Axon-Carrying Dendrites

The novel discovery on dendritic branches showing they can adjust themselves according to their roles is followed by a new discovery on dendrites. It is found that the axon can stem from basal dendrites in certain areas such as hippocampal CA3 and CA1 pyramidal neurons and a subset of cortical pyramidal cells in significant ratios (50% in CA1 pyramidal neurons and 30% in CA3 pyramidal neurons) (Figure 1.8) [7].

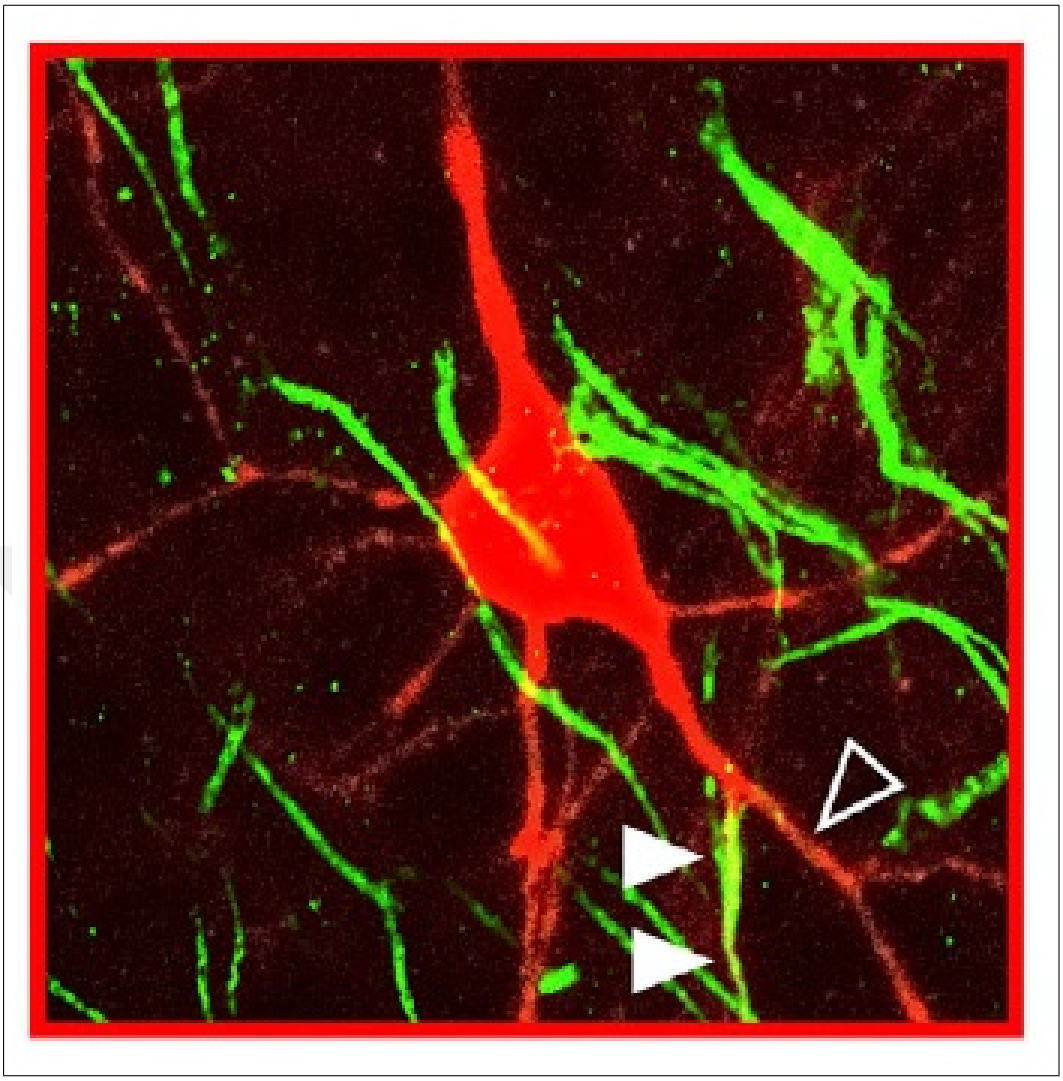

Figure 1.8 Axon originated from basal dendrite in CA1 pyramidal neuron (Soma and proximal dendrites were labeled with DsRed, axon is labeled with (AIS)-specific marker ankyrin-G) [7].

The first evidences of this feature (AcDs) were on rat pyramidal neurons in 1968 [42] followed by primate neocortex in 1979 [43]. Later it was shown that this phenomenon is not unique to pyramidal neurons as well. In fact, it is also found in neuroendocrine cells [44], dopaminergic neurons [45] and certain interneurons [46].

Dendrites can control EPSPs through the voltage-gated ion channels they have, alter the synaptic signals and their propagation and create local dendritic spikes, which triggers the axonal output for precise timing [47]. They enhance the stimulus selectivity, contribute to oriental tuning as well as inhibition of the stimulus in a complex manner

[48]. All these features in addition to modification of dendritic branch from basal dendrite instead of soma when needed shows the importance of the role of dendrites in synaptic information transmission; they do not only transfer the received input to soma, rather they work as small computational units of the neuron.

The findings on AcD put even more emphasis on the importance of dendrites in AP generation and EPSP & IPSP transmission. In the study which the AcDs are studied thoroughly in CA1 hippocampal pyramidal neurons, it was shown that AcDs have lower AP generation threshold and are more excitable compared to dendrites those do not carry axons [7].

1.4 Artificial Neurons

Neurons contain highly developed dendritic trees which may have length of several hundreds of μm and the dendritic trees contain the synaptic input. Electrical properties of neurons are similar to a capacitor which are charged by the synaptic input and ion currents. Rall model provides cable theory for multi-compartmental models [49], he showed that voltage attenuation is spread asymmetrically [50].

The models can be quite complicated when voltage dependent ionic conductances are also considered. High dimensional system of equations is needed to be solved by using multi-compartmental models as the numerical integration over the spatially discretized dendrites.

The general approach of a conductance-based model can be denoted as

$$C_m\dot{V}(t) = -i_m + I_{inj}/A \tag{1.1}$$

where C_m is the membrane capacitance, i_m is the membrane current and I_{inj}/A is the current injected per surface area.

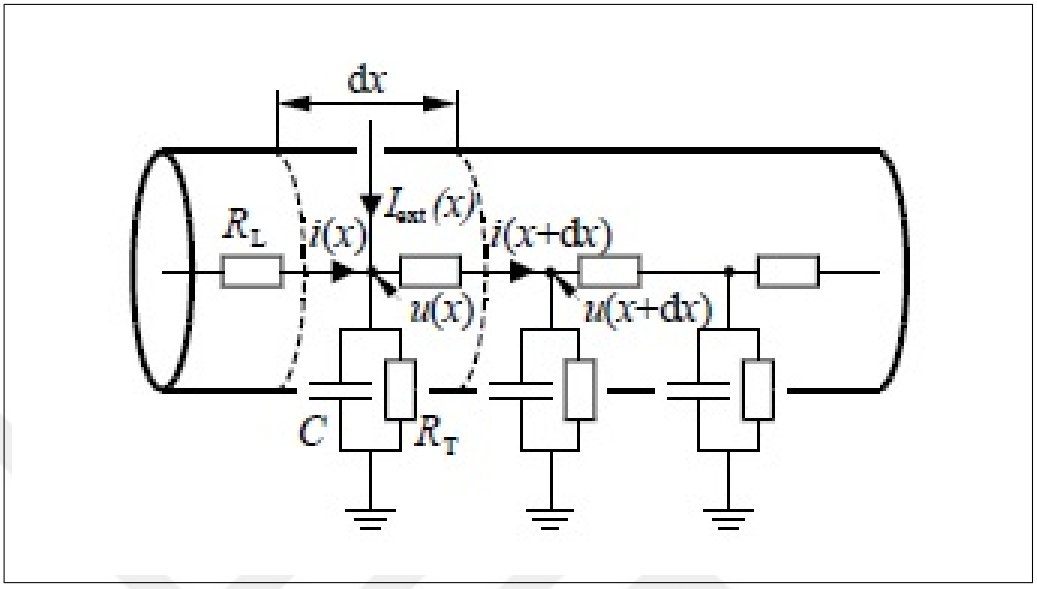

Figure 1.9 Neurite branch shown as a circuit diagram scheme. Electrical capacity of each part is denoted with C, longitudinal resistor as R_L, transversal resistor as R_T [8].

1.5 Hodgkin Huxley Model

The biophysical parameters of the modeled cells are based on Hodgkin-Huxley cell model. The Hodgkin-Huxley model is developed by Alan Lloyd Hodgkin and Andrew Huxley in 1952 with help of data collected from a squid giant axon. The model then led to a Nobel prize in 1963.

The model explains the ionic mechanisms in an excitable cell and further explains AP initiation and propagation. The model represents the cell with an electrical circuit and represents each compartment of the cell as a unit of this electrical circuit.

In the model, lipid bilayer cell membrane is represented as a capacitance. Voltage gated ion channels (Na^+ and K^+ channels) are represented as electrical conductances. Leak channels are represented as linear conductances. Electrochemical gradi-

ents that regulates the ion flow through membrane are represented as voltage sources. Ion pumps are represented as current sources. The units can be dependent on ionic concentrations as well as time or transmembrane potential [51].

$$I = C_m \frac{dV_m}{dt} + \overline{g}_K n^4 (V_m - V_K) + \overline{g}_{Na} m^3 h (V_m - V_{Na}) + \overline{g}_l (V_m - V_l) \tag{1.2}$$

$$m(t) = m_0(\upsilon_1) + [(m_0(\upsilon_0) - m_0(\upsilon_1))] e^{[-(t-t_0)/\tau m(\upsilon_1)]} \tag{1.3}$$

$$h(t) = h_0(\upsilon_1) + [(h_0(\upsilon_0) - h_0(\upsilon_1))] e^{[-(t-t_0)/\tau h(\upsilon_1)]} \tag{1.4}$$

$$n(t) = n_0(\upsilon_1) + [(n_0(\upsilon_0) - n_0(\upsilon_1))] e^{[-(t-t_0)/\tau n(\upsilon_1)]} \tag{1.5}$$

2. MATERIALS AND METHODS

In order to understand the concept of AcDs computational modeling is used. Computational modeling helps us to use various parameters, observe the changes and the outcomes in a complex manner in less amount of time. It also helps us to make predictions to be studied in the future on real cells or tissues.

The main purpose of the single cell models is to analyze the differences between AcDs and nonAcDs. AcDs are found abundantly in hippocampal CA1 and CA3 pyramidal neurons.

Another reason for choosing hippocampal CA1 and CA3 pyramidal neurons is their connection. Since these cells are very similar, located in the same structure and interact each other frequently in trisynaptic loop, it is more reliable to compare both axon carrying and nonAcDs in CA1 and CA3 pyramidal cells.

These cells are very hard to separate and examine on live tissues. The cells begin to deteriorate soon after the brain extraction process. In order to detect the cells, they have to undergo chemical processes. After this chemical process even though the cells are still alive, there will be too many variables to make a solid comparison statement.

Because of this difficulty, realistic cell models are used to examine the variables. However, realistic models also have their own difficulties. There are too many variables in living cells that it is almost impossible to put every variable in a cell model. However, neurons act as small electrical circuits that convert analog input to digital output, thus determining the essential parameters of this circuit (i.e. conductance, resistance, threshold) gives a good estimate about the neuron's characterization.

For the models, cell geometries are designed by analysis of real CA1 and CA3 pyramidal cells [4]. For the biophysical properties, Hodgkin-Huxley model is applied

with the implementation of Na_v and K_v channels. However, the biophysical parameters had to be simpler compared to the real pyramidal cells for 2 reasons. Firstly, we want to observe the effect of AcD geometry with the simplest conductance-based model possible. With the increasing number of parameters, the results would be hard to interpret with large number of variables.

2.1 Softwares

2.1.1 NEURON 7.5

For modeling the cells NEURON 7.5 simulation environment is used. It comes with a graphic user interface which is also interpretable by Neuron's programming language hoc as well as Python. NEURON is developed by researchers at Yale University in 1976 and with the help of being an open source program, it is still being developed by researchers all around.

The major advantage of this program is that the cells can be studied simulating the culture i.e. the patch-clamp recordings can be simulated realistically. Both single cell and network modeling can be done with the program. The users can formulate a conceptual model, implement models into NEURON environment, set and run simulations and analyze the results using NEURON program [52]. As of 2018, more than 580 models generated with NEURON program is open to access in Model DB.

Since it is a specific program for neurons and neural networks, the users can analyze electrical and chemical signaling with active membrane properties (transmembrane currents, transmembrane channels) in models with realistic geometry. It takes the neurites and soma as segments and formulates according to this, so that the biophysical and biochemical dynamics of synaptic transmission can be observed through time. Compartmentalization provides reduction of cable equation to a set of ordinary differential equations with first order derivatives in time. The algebraic difference equations can be solved numerically with temporal discretization afterwards. The electronic

and active signaling along the dendritic branches and axonal cable can be measured regardless of the dendritic branch complexity. In NEURON program forward Euler method, backward Euler method and Crank-Nicholson method is used for numerical integration [53].

2.1.2 MATLAB r2017b

Results of the simulations are analyzed with MATLAB r2017b Academic use, developed by Mathworks. It is one of the world's most widely used product for algorithmic development with over 1 million users [54]. It allows users to manipulate matrices, plotting data and functions, implementation of algorithms. Users can also create their own user interfaces since it is integrable with a wide range of programming languages including Python, Java, C, C++, C# and Fortran.

2.2 Model Setup

Geometrical Parameters

Multicompartmental cell model is used for single cell models. This kind of models estimate the cellular biophysics by dividing the cell into numerous cylindrical compartments. Each compartment may have different conductance properties. Even the dendrites which are the most non-uniform parts of a neuron can be locally evaluated as a uniform cable [55].

The cells are designed to be highly symmetrical to eliminate the errors or deviations in the results that can stem from geometrical differences. For this purpose, the only difference between axon-carrying CA1 and regular CA1 cell models (just as axon carrying CA3 and regular CA3 cell models) is the basal dendritic branch on the left hand side. In AcDs, there is one basal dendrite that is connected to the axon hillock and carries the axon. In regular cell models there are two basal dendrites that stem

from a small arm connected to soma, the same structure of the basal dendrites on the right-hand side.

The biophysical parameters are kept as similar as possible to real CA1 and CA3 pyramidal neurons from the tip of the apical dendrite to the axon terminal. Real CA1 pyramidal neurons are found to be 730μm and real CA3 pyramidal neurons are found to be 580μm [4]. In this model cell length is determined accordingly. As can be seen in Figure 1.4 apical dendrites of CA3 pyramidal neurons branch closer to soma whereas in CA1 pyramidal neurons the apical dendrite is more distinctive. To project this difference, apical tuft of CA1 pyramidal cells are adjusted to 70μm while it is kept at 150μm in CA3 pyramidal cells.

The apical dendrite (the section from soma to apical tuft) is divided into 3 subgroups and notated as proximal, medial and distal respectively. Since this section is smaller in CA3 pyramidal cells, they are kept as 5μm, 5μm and 5μm in both axon carrying and regular CA3 pyramidal cell models. On the other hand, this section is longer in CA1 pyramidal cells, the apical tuft starts further away from soma. The proportions are kept as similar as possible to the real cell values and the proximal, medial, distal parts are kept as 40μm, 40μm and 40μm respectively in both axon carrying and regular CA1 pyramidal neuron models. The diameters of proximal, medial, distal and LM in all 4 cell models are 4,3,2,2 respectively [7], starting with wider width and decreasing as the compartment is further away from soma.

Soma of axon carrying and regular CA1 pyramidal neuron is round and has 30μm diameter according to the cell model in article of Thome et al. [7]. Since CA3 pyramidal neuron somata are bigger, their diameters are determined as 40μm in both axon carrying and regular CA3 pyramidal neurons. Leakage reversal potential is kept at -70 mV for all of the compartments.

Biophysical Parameters

For biophysical parameters paper on AcDs of Thome et al. is used as reference and adjusted. The model cells are tried to be kept as simple as possible to have minimum parameters because, the effect of only the geometrical difference is wanted to be shown. The single cell models did not make any synapses and they are examined by their AP characteristics and their potential propagation properties. For this purpose, calcium channels are omitted.

The compartments have 200 Ω-cm axial resistance [56]. Membrane capacitance is determined as 1 μF/cm^2 in each segment but soma in which, the membrane capacitance is determined as 1.1 μF/cm^2. Myelins are determined to have only passive channels. Sodium channel density is determined to be denser in and node of ranviers 10 fold compared to soma and sparse in apical dendrite. Potassium channel density is determined to be 0.036 μF/cm^2 and leak channel density is determined to be 0.0003 μF/cm^2 in each segment except myelinated segments.

The biophysical properties are kept the same for all of the four cell models. The only difference between axon carrying and regular cells and CA1 and CA3 cells is their geometrical differences.

2.2.1 CA1 Pyramidal Neuron With AcD

The geometry of the CA1-AcD cell, the topological properties and biophysical properties of each compartment is shown below.

Table 2.1
Geometrical properties of CA1 hippocampal pyramidal cells with AcD.

	L(μm)	Diam (μm)
Lms	70	2
Distal	40	2
Medial	40	3
Proximal	40	4
Soma	30	30
xxs	5	1.5
basals	100	1.4
ais	40	1.22
myelins	50	1
NRs	2	1
ah	5	1.5
bleb	2	2

Table 2.2
Biophysical properties of CA1 hippocampal pyramidal cells with an AcD.

	Ra (Ω-cm)	Cm (μF/cm^2)	$\overline{gNa}$ (S/cm^2)	$\overline{gK}$ (S/cm^2)	$\overline{gl}$ (S/cm^2)	El (mV)
Lms	200	1	0.005	0.036	0.0003	-70
Distal	200	1	0.005	0.036	0.0003	-70
Medial	200	1	0.005	0.036	0.0003	-70
Proximal	200	1	0.05	0.036	0.0003	-70
Soma	200	1.1	0.05	0.036	0.0003	-70
Xxs	200	1	0.05	0.036	0.0003	-70
Basals	200	1	0.05	0.036	0.0003	-70
Ais	200	1	0.5	0.036	0.0003	-70
Myelins	200	1	-	-	-	-70
NRs	200	1	0.5	0.036	0.0003	-70
Bleb	200	1	0.05	0.036	0.0003	-70

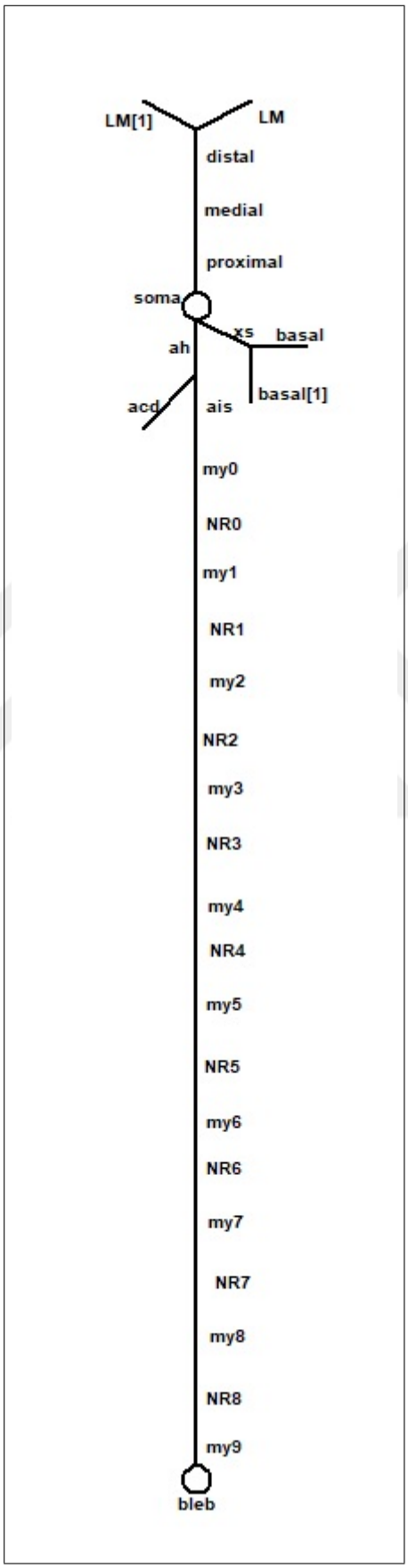

Figure 2.1 Hippocampal CA1 Pyramidal Cells with AcD topography.

2.2.2 CA1 Pyramidal Neuron With Regular Axon and Dendrites

The geometry of the CA1-nonAcD cell, the topological properties and biophysical properties of each compartment is shown below.

Table 2.3
Geometrical properties of CA1 hippocampal pyramidal cells with regular axon and dendrites.

	L(μm)	Diam (μm)
Lms	70	2
Distal	40	2
Medial	40	3
Proximal	40	4
Soma	30	30
xxs	5	1.5
basals	100	1.4
ais	40	1.22
myelins	50	1
NRs	2	1
bleb	2	2

Table 2.4
Biophysical properties of CA1 hippocampal pyramidal cells with regular axon and dendrites.

	Ra (Ω-cm)	Cm (μF/cm^2)	$\overline{gNa}$ (S/cm^2)	$\overline{gK}$ (S/cm^2)	$\overline{gl}$ (S/cm^2)	El (mV)
Lms	200	1	0.005	0.036	0.0003	-70
Distal	200	1	0.005	0.036	0.0003	-70
Medial	200	1	0.005	0.036	0.0003	-70
Proximal	200	1	0.05	0.036	0.0003	-70
Soma	200	1.1	0.05	0.036	0.0003	-70
Xxs	200	1	0.05	0.036	0.0003	-70
Basals	200	1	0.05	0.036	0.0003	-70
Ais	200	1	0.5	0.036	0.0003	-70
Myelins	200	1	-	-	-	-70
NRs	200	1	0.5	0.036	0.0003	-70
Bleb	200	1	0.05	0.036	0.0003	-70

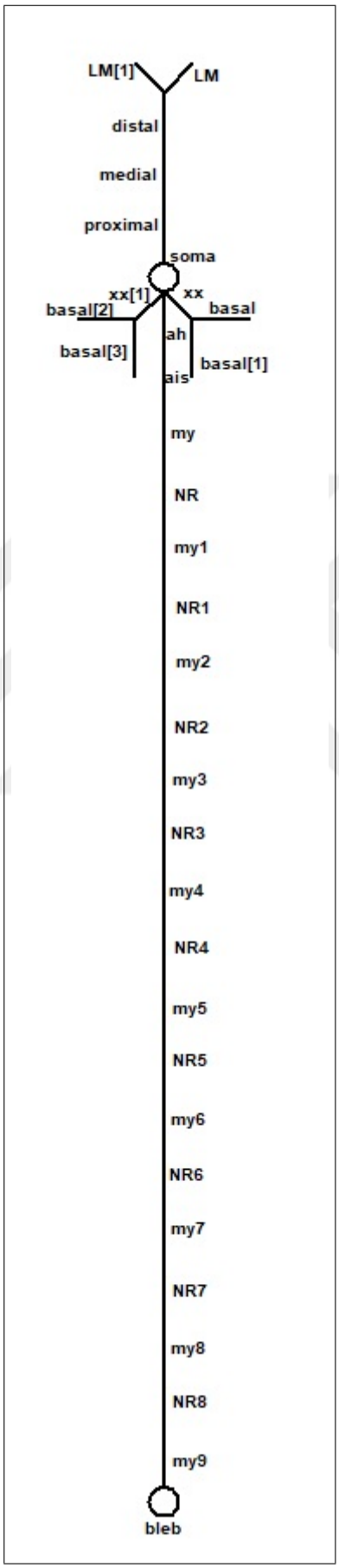

Figure 2.2 Hippocampal CA1 Pyramidal Cells with Regular Axon and Dendrite Topography.

2.2.3 CA3 Pyramidal Neuron With AcD

The geometry of the CA3-AcD cell, the topological properties and biophysical properties of each compartment is shown below.

Table 2.5
Geometrical properties of CA3 hippocampal pyramidal cells with AcD.

	L(μm)	Diam (μm)
Lms	150	2
Distal	5	2
Medial	5	3
Proximal	5	4
Soma	40	40
xxs	5	1.5
basals	100	1.4
ais	40	1.22
myelins	50	1
NRs	2	1
bleb	2	2

Table 2.6
Biophysical properties of CA3 hippocampal pyramidal cells with AcD.

	Ra (Ω-cm)	Cm (μF/cm^2)	$\overline{gNa}$ (S/cm^2)	$\overline{gK}$ (S/cm^2)	$\overline{gl}$ (S/cm^2)	El (mV)
Lms	200	1	0.005	0.036	0.0003	-70
Distal	200	1	0.005	0.036	0.0003	-70
Medial	200	1	0.005	0.036	0.0003	-70
Proximal	200	1	0.05	0.036	0.0003	-70
Soma	200	1.1	0.05	0.036	0.0003	-70
Xxs	200	1	0.05	0.036	0.0003	-70
Basals	200	1	0.05	0.036	0.0003	-70
Ais	200	1	0.5	0.036	0.0003	-70
Myelins	200	1	-	-	-	-70
NRs	200	1	0.5	0.036	0.0003	-70
Bleb	200	1	0.05	0.036	0.0003	-70

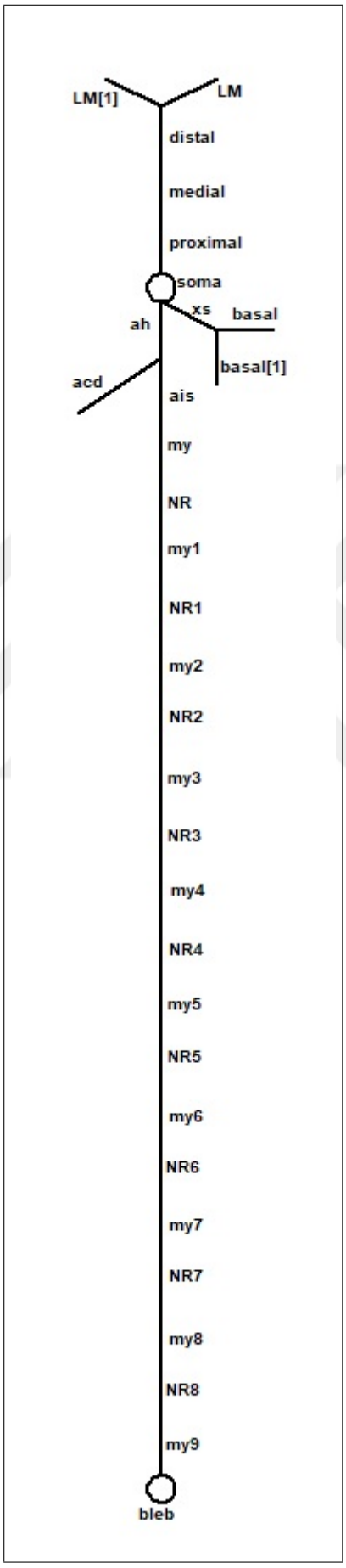

Figure 2.3 Hippocampal CA3 Pyramidal Cells with ACD Topography.

2.2.4 CA3 Pyramidal Neuron With Regular Axon and Dendrites

The geometry of the CA3-nonAcD cell, the topological properties and biophysical properties of each compartment is shown below.

Table 2.7
Geometrical properties of CA3 hippocampal pyramidal cells with regular axon and dendrites.

	L(μm)	Diam (μm)
Lms	150	2
Distal	5	2
Medial	5	3
Proximal	5	4
Soma	40	40
xxs	5	1.5
basals	100	1.4
ais	40	1.22
myelins	50	1
NRs	2	1
bleb	2	2

Table 2.8
Biophysical properties of CA3 hippocampal pyramidal cells with regular axon and dendrites.

	Ra (Ω-cm)	Cm (μF/cm^2)	$\overline{gNa}$ (S/cm^2)	$\overline{gK}$ (S/cm^2)	$\overline{gl}$ (S/cm^2)	El (mV)
Lms	200	1	0.005	0.036	0.0003	-70
Distal	200	1	0.005	0.036	0.0003	-70
Medial	200	1	0.005	0.036	0.0003	-70
Proximal	200	1	0.05	0.036	0.0003	-70
Soma	200	1.1	0.05	0.036	0.0003	-70
Xxs	200	1	0.05	0.036	0.0003	-70
Basals	200	1	0.05	0.036	0.0003	-70
Ais	200	1	0.5	0.036	0.0003	-70
Myelins	200	1	-	-	-	-70
NRs	200	1	0.5	0.036	0.0003	-70
Bleb	200	1	0.05	0.036	0.0003	-70

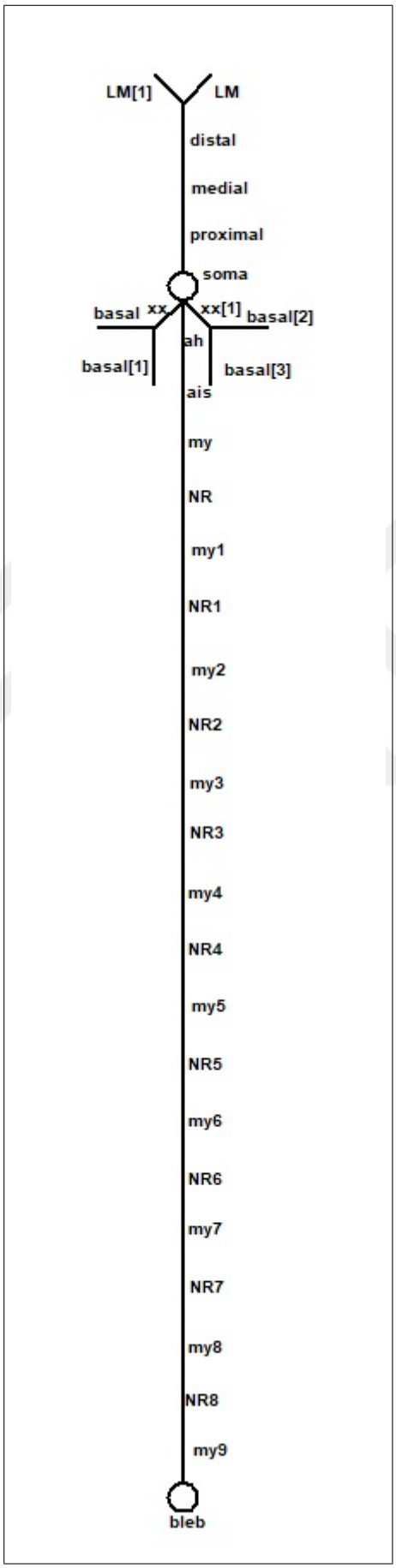

Figure 2.4 Hippocampal CA3 Pyramidal Cells with Regular Axon and Dendrite Topography.

2.2.5 Current Injection

The only stimulant in the model cells is the current injection. The cells do not make any synapses. Current injection is selected by "electrode" section under the point process manager menu. The applied section is determined as "soma (0.5)", the middle of soma. The injection started with 5 ms delay to examine the AP initiation with detail. The recordings are stopped 5 ms after the AP. Total duration of the recordings are 30 ms.

The minimum required AP is determined by increasing 0.1 nA and then adjusted to 4 significant figure precisions. This process is repeated for the models without dendritic branches. The stable current is determined by comparing the minimum currents required for model cells to initiate AP. The maximum current needed was CA3-nonAcD model cell with 0.5666 nA.

2.3 Data Analysis

2.3.1 Action Potentials

After the current injection to soma, potential changes are recorded from each compartment with 0.025s time increments from all the compartments. Data was extracted as potential traces from each compartment and analyzed in Matlab (v.r2017b)

2.3.2 Phase Plots

The rate of potential change was estimated by the first derivative of potentials (dV/dt), normalized by 0.025 ($\triangle t$). $\dot{V}$ vs. V was displayed as phase plots.

2.3.3 Delay

The distance of each segment from AIS ($x = 0$) was estimated from the midpoint of each segment. The delay and the attenuation with respect to distance from AIS. The delay was estimated as

$$\triangle t_{peak} = t_{peak,x} - t_{peak,AIS} \tag{2.1}$$

$t_{peak,AIS}$ is the time of AP peak point of AIS, $t_{peak,x}$ is the time of AP peak of corresponding segment and $\triangle t_{peak}$ is the delay between AP peaks.

The results were displayed in $\triangle t_{peak}$ vs. distance plots.

2.3.4 Steepness

AP steepness was either estimated as maximum steepness ($\ddot{V}_{max}$) or threshold steepness ($\ddot{V}_{thr}$) by taking the second derivative of potential trace (V). ($\ddot{V}_{max}$) is the actual steepness of AP onset for each segment, whereas ($\ddot{V}_{thr}$) is the steepness of each segment at threshold passing ($\ddot{V}_{thr,AIS}$).

($\ddot{V}_{max}$) shows how fast the AP reaches to its maximum point thus, the responsiveness of the compartments whereas, ($\ddot{V}_{thr}$) shows the relation of compartmental ($\ddot{V}$) with respect to distance from AIS.

2.3.5 FI Curves

To understand the response characteristics of the cells, FI curves are plotted. To plot the FI Curves, the I_{min}/cm^2 is used as the starting current point. The current is applied for 1 second and number of APs are recorded in 1 s timescale. The current is increased by 0.5 nA increments. When the repetitive firing pattern is reached, 0.1

nA increments are added starting with the previous current point. The number of peaks is noted until the increase in the number of APs starts slowing down. Then the increments are increased to 0.5 nA again, until the model cell is saturated.

The saturation is determined by the shape of the APs. The AP loses its shape and a sinusoidal wave is seen as a tetanic response to the given high current. At that point the measurement is stopped

3. RESULTS

3.1 Neural Response to Minimum Current Injection

After the model cells were designed, minimum current required for the cells to fire an AP (I_{min}) was measured. I_{min} was applied at the center of the soma and was determined by increasing the amplitude by small increments until 4 significant number precisions.

3.1.1 Action Potential Thresholds

Minimum current necessary for the model cells to fire an AP was noted as I_{min} for each cell and given in Table 3.1.

Table 3.1
Minimum current injections required for model cells to initiate an AP.

	AcD	Non-AcD
CA1	0.3911 nA	0.4275 nA
CA3	0.5289 nA	0.5666 nA

I_{min} amplitudes were found to be lower in AcD cells compared to nonAcD cells. CA1 neurons required less I_{min} than the CA3 models.

3.1.2 Action Potential Waveforms

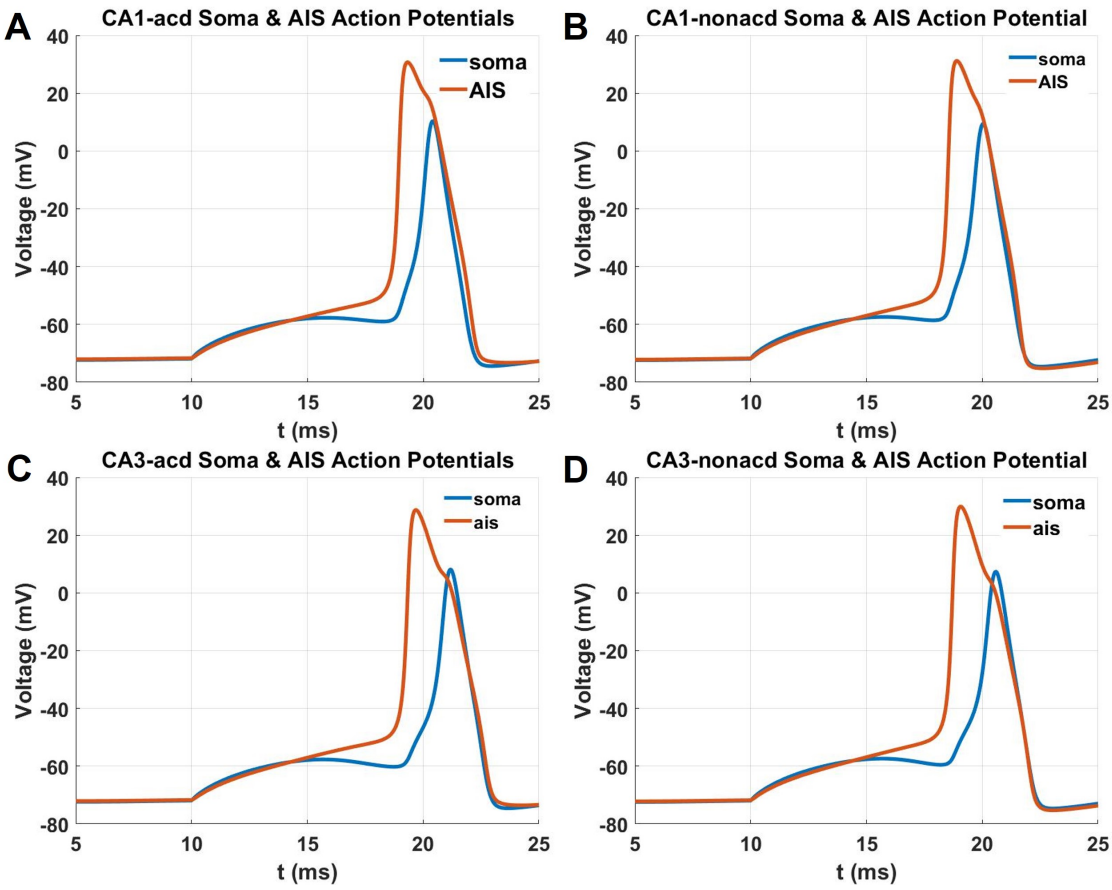

Figure 3.1 APs of soma and AIS of the model cells with I_{min}. (A)AP of CA1-AcD soma and AIS, (B)AAP of CA1-nonAcD soma and AIS, (C)AP of CA3-AcD soma and AIS, (D)AP of CA3-nonAcD soma and AIS.

AP waveforms of soma and AIS are examined in detail. The reason for choosing these two compartments is, AIS is the compartment that AP is initiated, and soma is the compartment where the electrophysiological activity of the cell is generally recorded. The AP waveforms of the AcD cells and nonAcD cells did not show a significant difference. All the cells have a sharply increasing AP in the AIS. The APs of both CA3 cells (both in AcD and non-AcD) have slightly lower peak potential compared to CA1 (both in AcD and nonAcD) cells.

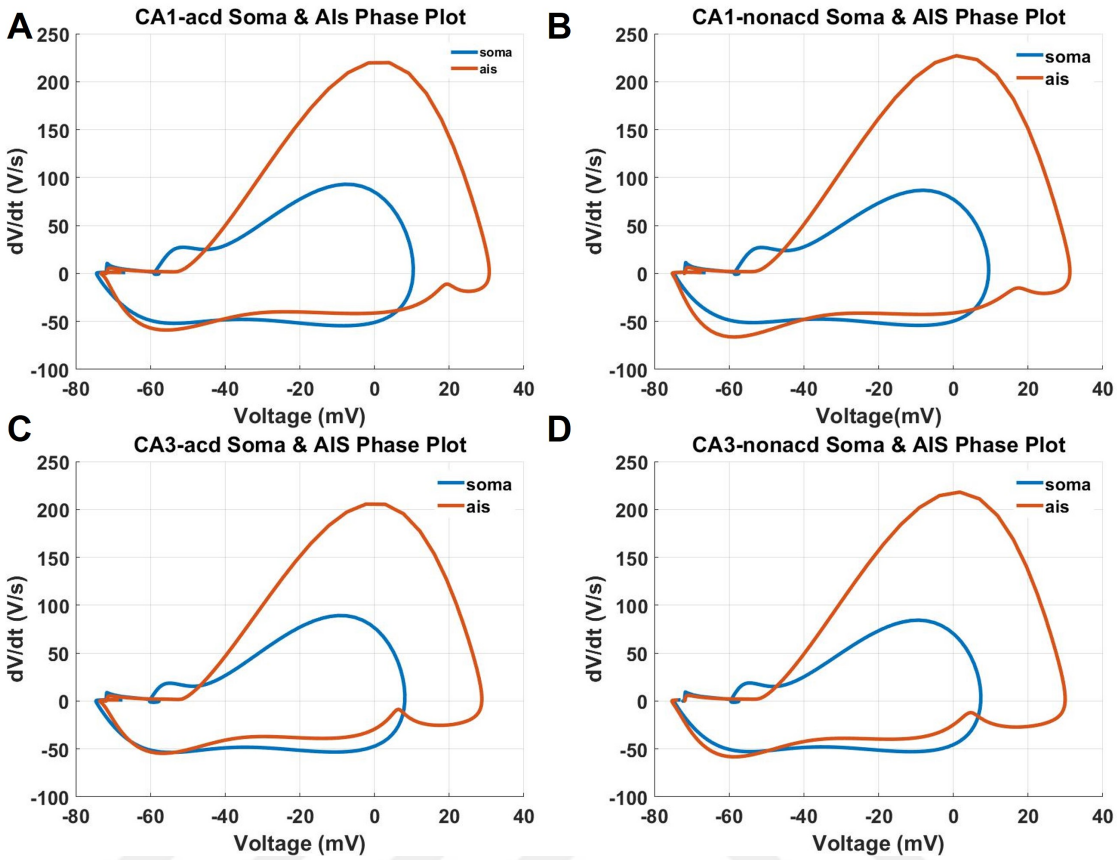

Figure 3.2 Phase plots of AIS and soma of the cells with APs of soma and AIS of the cells with I_{min} injection (A) Phase plot of CA1-AcD AIS and soma (B)Phase plot of CA1-nonAcD AIS and soma (C)Phase plot of CA3-AcD AIS and soma (D)Phase plot of CA3-nonAcD AIS and soma.

Phase plots show the acceleration of the APs by plotting the potential difference in time at the given potential. The plots are similar when AcD and nonAcD cells are compared. The differences between CA1 and CA3 cells are expected because of the geometrical differences of their soma.

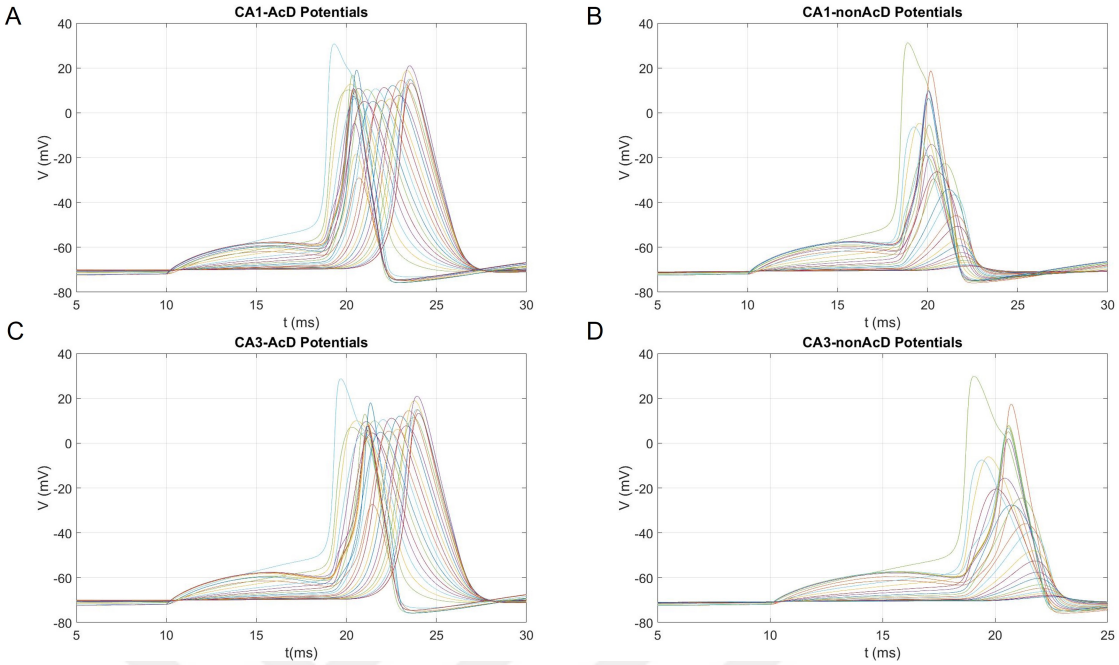

Figure 3.3 Potential waveforms of the cells with I_{min} injection (A) Potential waveforms of CA1-AcD (B)Potential waveforms of CA1-nonAcD (C)Potential waveforms of CA3-AcD (D)Potential waveforms of CA3-nonAcD.

The potential waveforms collected from each segment of the cells show quite distinctive properties. To understand the causality, the cells are further analyzed according to their distance, delay or steepness properties.

3.1.3 Action Potential Propagation

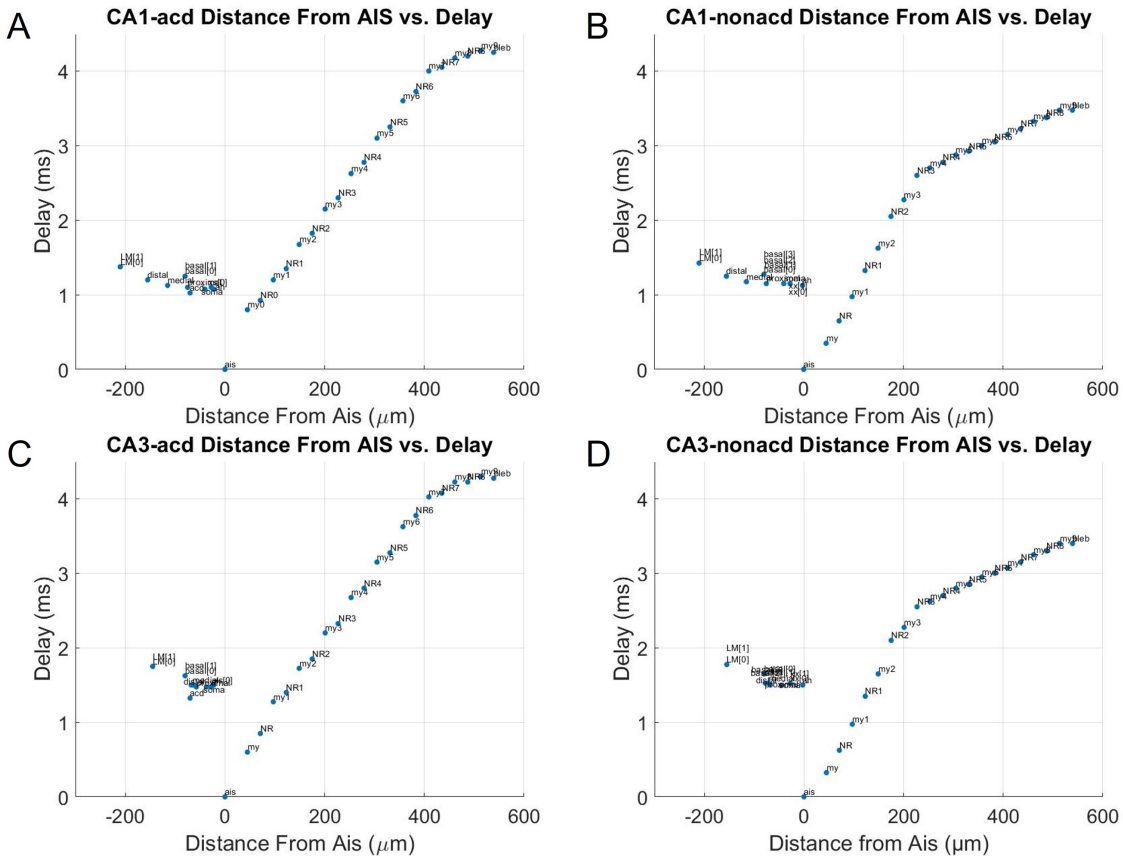

Figure 3.4 Distance from AIS vs. delay of V_{max} of compartments with I_{min} injection (A) Distance vs. Delay plot of CA1-AcD cell (B)Distance vs. Delay plot of CA1-nonAcD cell (C)Distance vs. Delay plot of CA3-AcD cell (D)Distance vs. Delay plot of CA3-nonAcD cell.

Time differences between the peak points of APs of each segment is measured and compared according to their distance from AIS. According to the plot, AcD cells are slower in AP propagation to bleb compared to nonAcD cells. However, propagation of potential to basal dendrites and apical dendrites are slower in nonAcD cells. The precise time differences can be found in Table A.1, Table A.2, Table A.3 and Table A.4.

CA1 cells required less time to propagate potential to other compartments compared to CA3 cells in both AcD and nonAcD cells. The trends in propagation is consistent in both AcD and nonAcD cells.

3.1.4 Onset Steepness

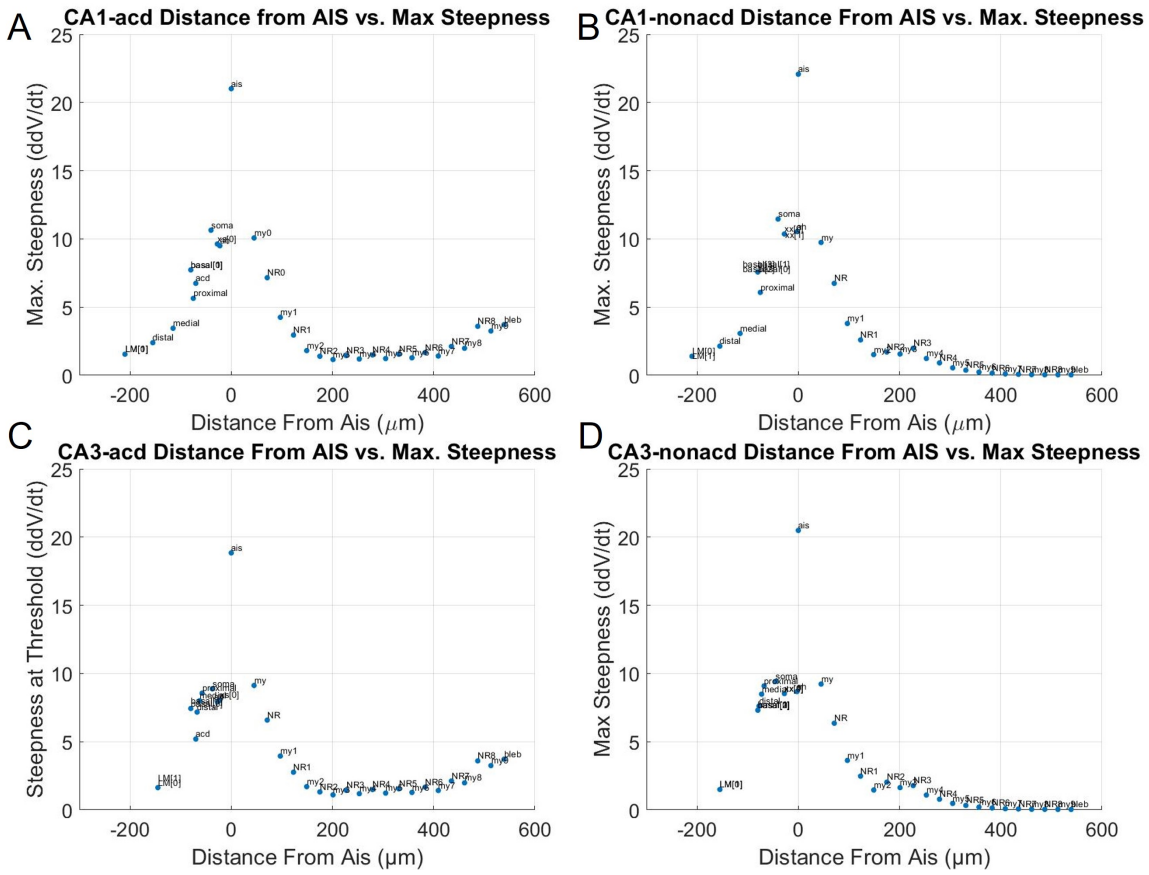

Figure 3.5 $\ddot{V}_{max}$ of each compartment according to their distance from AIS with I_{min} injection (A) Distance from AIS vs. $\ddot{V}_{max}$ of each compartment of CA1-AcD according to their distance from AIS with I_{min} injection (B)Distance from AIS vs. $\ddot{V}_{max}$ of each compartment of CA1-nonAcD according to their distance from AIS with I_{min} injection (C)Distance from AIS vs. $\ddot{V}_{max}$ of each compartment of CA3-AcD according to their distance from AIS with I_{min} injection (D)Distance from AIS vs. $\ddot{V}_{max}$ of each compartment of CA3-nonAcD according to their distance from AIS with I_{min} injection.

$\ddot{V}_{max}$ of the compartments are calculated by taking second derivative of the potential values that the compartments reach. It shows the responsiveness of the compartments. According to the plots AcD models have lower $\ddot{V}_{max}$ in AIS compared to nonAcD cells. The AcD cells have higher $\ddot{V}_{max}$ amplitudes compared to nonAcD cells in compartments close to axon terminal. In nonAcD cells the $\ddot{V}_{max}$ amplitude decreases in compartments closer to axon terminal.

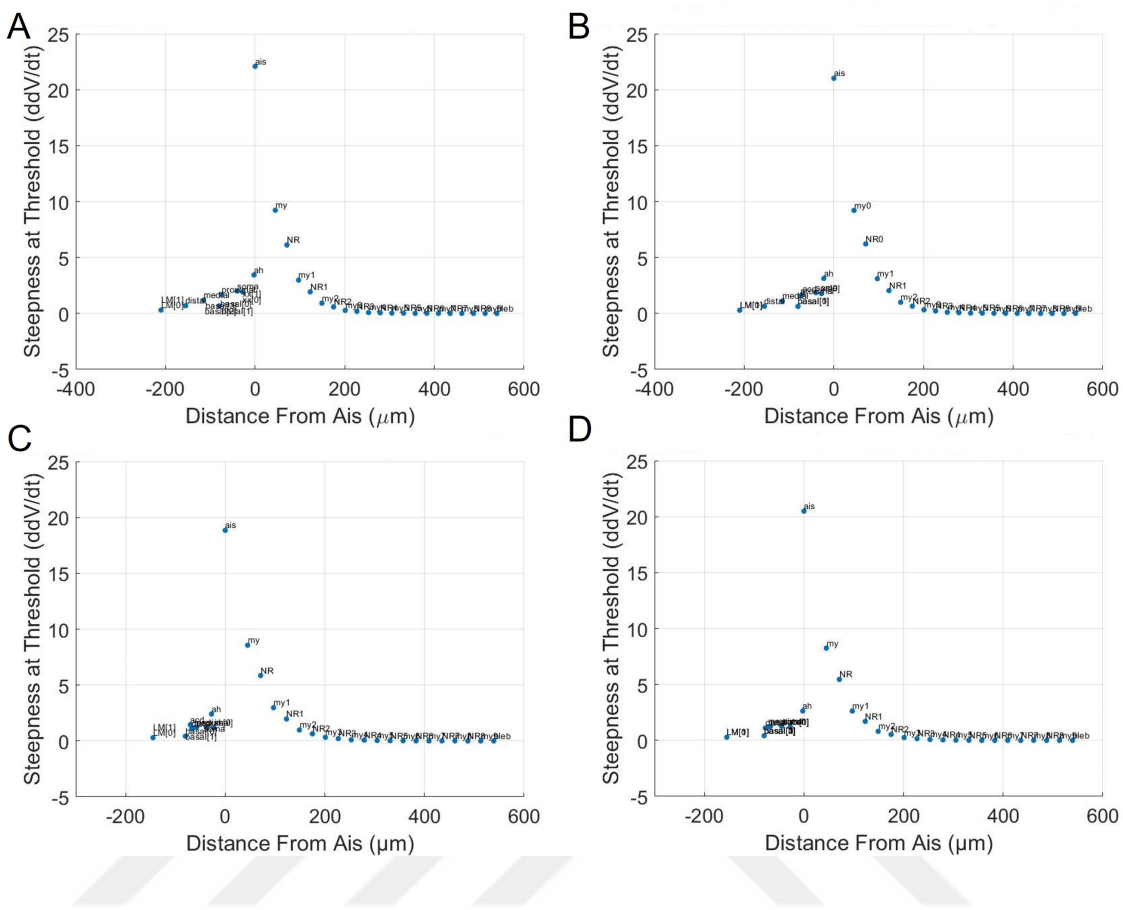

Figure 3.6 Distance from AIS vs. $\ddot{V}_{thr}$ of each compartment at the time $\ddot{V}_{max}$ of AIS is at its maximum with I_{min} (A) Distance from AIS vs. $\ddot{V}_{thr}$ of CA1-AcD cell. (B)Distance from AIS vs. $\ddot{V}_{thr}$ values of CA1-nonAcD cell. (C)Distance from AIS vs. $\ddot{V}_{thr}$ values of CA3-AcD cell. (D)Distance from AIS vs. $\ddot{V}_{thr}$ values of CA3-nonAcD cell.

$\ddot{V}_{thr}$ plot shows the steepness of each compartment at the time $\ddot{V}_{max}$ of AIS is at its maximum with I_{min} injection. This plot shows the responsiveness of the compartments with respect to AIS. Higher $\ddot{V}_{thr}$ in the neighboring compartments show higher response to AP in the AIS. The plot shows similar responses from the compartments in each cell.

3.1.5 Vmax

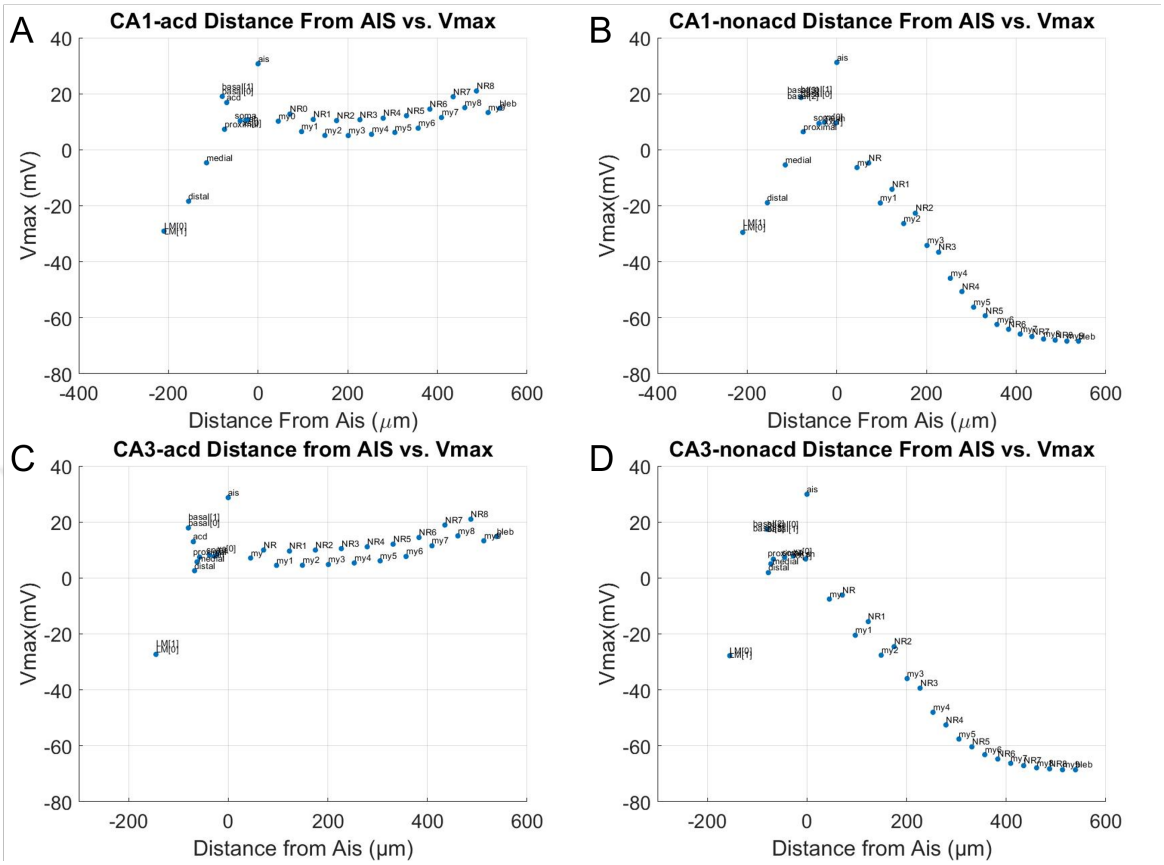

Figure 3.7 Distance from AIS vs. V_{max} of each compartment with I_{min} injection (A) Distance from AIS vs. V_{max} of CA1-AcD cell. (B)Distance from AIS vs. V_{max} of CA1-nonAcD cell. (C)Distance from AIS vs. V_{max} of CA3-AcD cell. (D)Distance from AIS vs. V_{max} of CA3-nonAcD cell.

V_{max} of each segment is plotted versus their distance to AIS. This plot shows that the peak potential amplitude decreases as the potential is propagated along the axon in nonAcD cells. On the contrary, in AcD cells, the peak potential amplitude is conserved. Peak potential amplitude of AIS is similar when the AcD and nonAcD cells are compared.

The proximal, medial and distal compartments of CA3 cells have higher peak potential values.

3.1.6 FI Curves

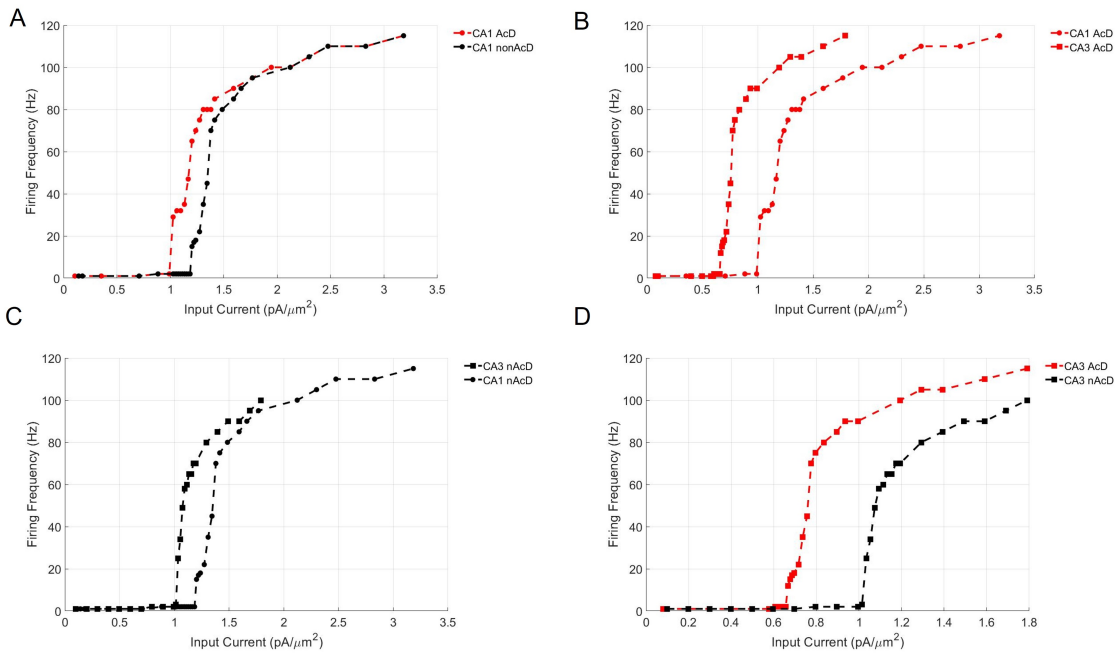

Figure 3.8 FI curve comparisons of the cells with I_{inj} injection (A)FI curve comparison of CA1-AcD and CA1-nonAcD cells (B)FI curve comparison of CA1-AcD and CA3-AcD cells (C)FI curve comparison of CA1-nonAcD and CA3-nonAcD cells (D)FI curve comparison of CA3-AcD and CA3-nonAcD cells.

The first plot shows the latency of CA1-nonAcD compared to CA1-AcD however, they align in high current applications. In the second plot, we can see that the response of CA3-AcD is lower than CA1-AcD. Also the breakpoint of CA1-AcD indicates that it starts tetanic response earlier than CA3-AcD cell. When the non-AcD cells are examined, we see the opposite; CA3-nonAcD cell starts tetanic response earlier than CA1-nonAcD cell and CA1-nonAcD cell shows a latency. In the fourth plot where the CA3-AcD and CA3-nonAcD cells are compared, AcD cell gives an early response in alignment with the CA1 cells. In CA3 cells, the AcD and nonAcD cells do not overlap as in CA1 cells.

3.2 Stable Current

In order to eliminate the differences that can stem from low current, the same current of 0.6 nA (denoted as $I_{0.6}$) is applied on the soma to the single cell models. The injected current is determined according to the maximum of I_{min}, which belongs to CA3-nonAcD pyramidal cell model (0.5666 nA).

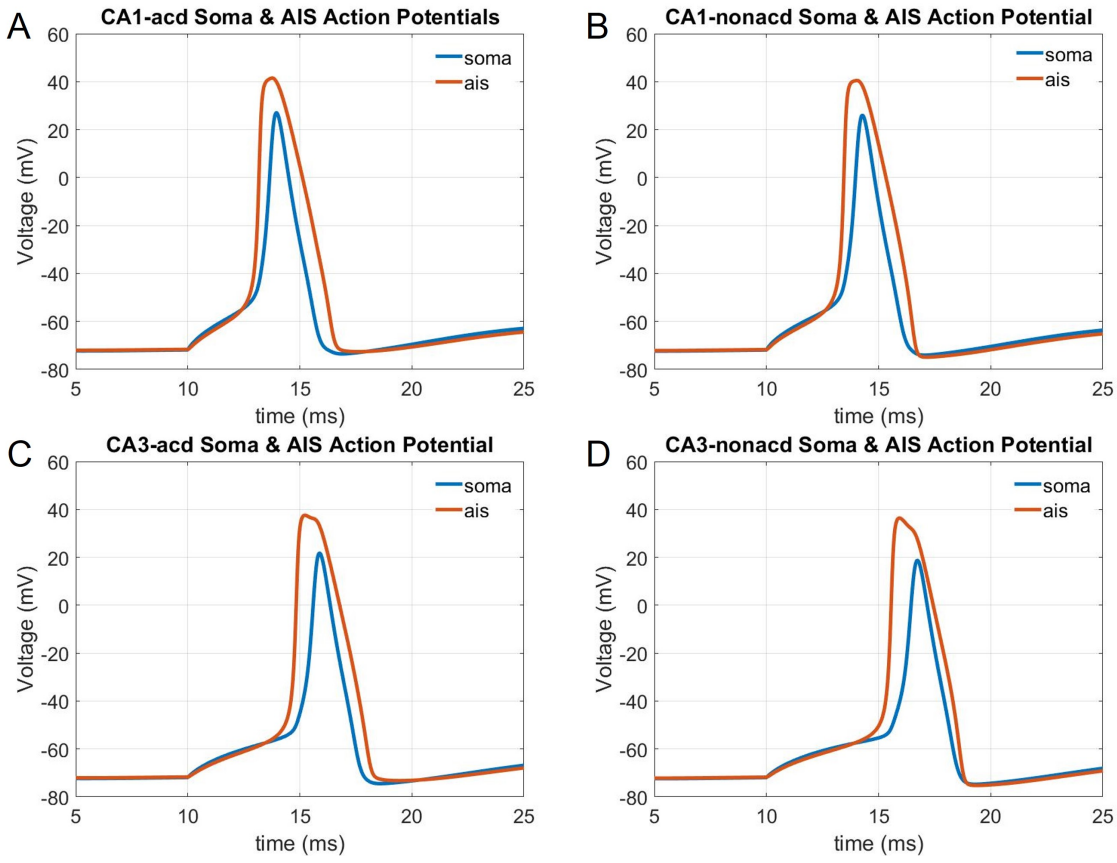

Figure 3.9 APs of soma and AIS of the model cells with 0.6 nA injected current. (A)AP of CA1-acd soma and AIS, (B)AP of CA1-nonacd soma and AIS, (C)AP of CA3-acd soma and AIS, (D)AP of CA3-nonacd soma and AIS.

When $I_{0.6}$ is injected to each cell, AcD cells had slightly higher peak points in AIS compared to AIS of nonAcD cells. CA3 cells are found to have a shoulder on the peak points of AIS. This shoulder is more observable in CA3-nonAcD AIS peak potential point compared to CA3-AcD AIS peak potential point.

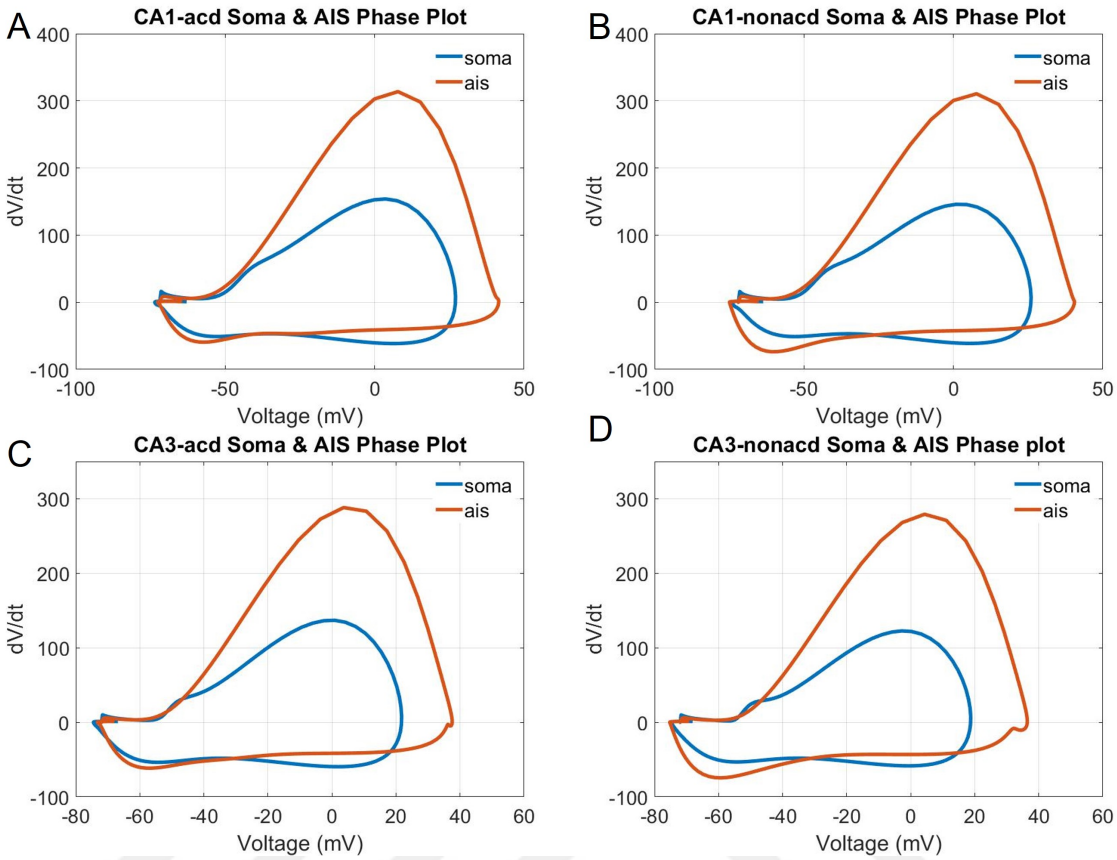

Figure 3.10 Phase plots of AIS and soma compartments of the cells with $I_{0.6}$ injection (A) Phase plot of CA1-AcD AIS and soma (B)Phase plot of CA1-nonAcD AIS and soma (C)Phase plot of CA3-AcD AIS and soma (D)Phase plot of CA3-nonAcD AIS and soma.

The AP properties of cells can be observed in more detail with the phase plots. AP peak points of both soma and AIS is higher in CA1-AcD and CA3-AcD models compared to CA1-nonAcD and CA3-nonAcD cells. The shoulder on top of the AIS of CA3 cells can be observed in more detail.

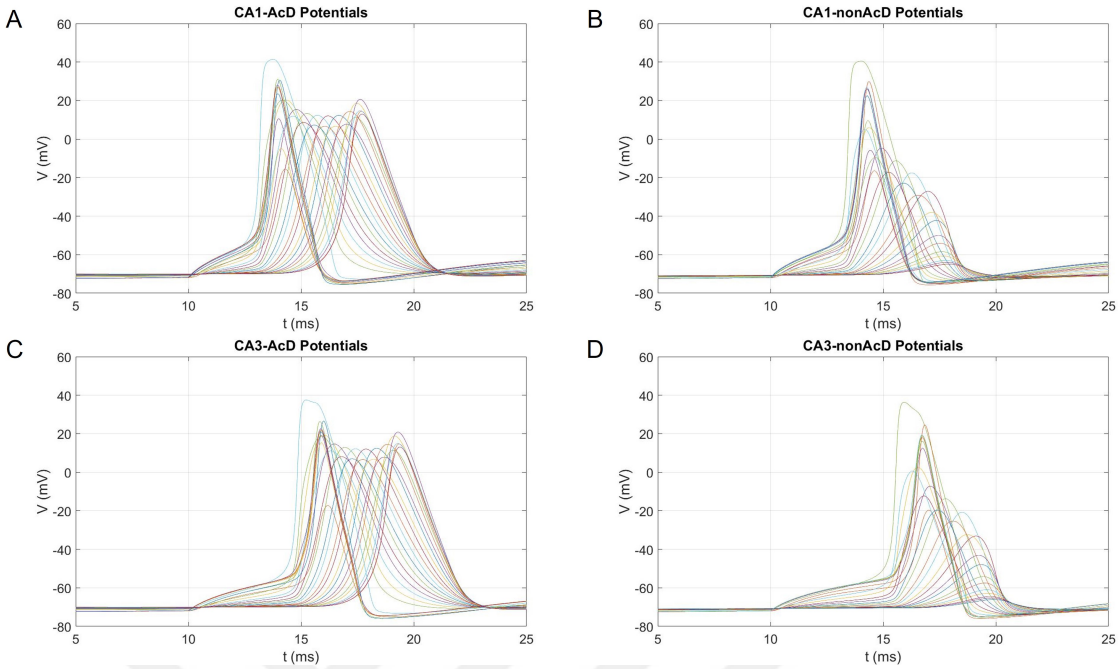

Figure 3.11 Potential waveforms of the cells with I_{min} injection (A) Potential waveforms of CA1-AcD (B)Potential waveforms of CA1-nonAcD (C)Potential waveforms of CA3-AcD (D)Potential waveforms of CA3-nonAcD.

The potential waveforms of each compartment of the cells can be observed from the Figure 3.11. The trend differences in the potential waveforms of AcD and nonAcD cells did not change with the higher current injection. The characteristics of the potential waveforms are further analyzed by examining their steepness and delay properties.

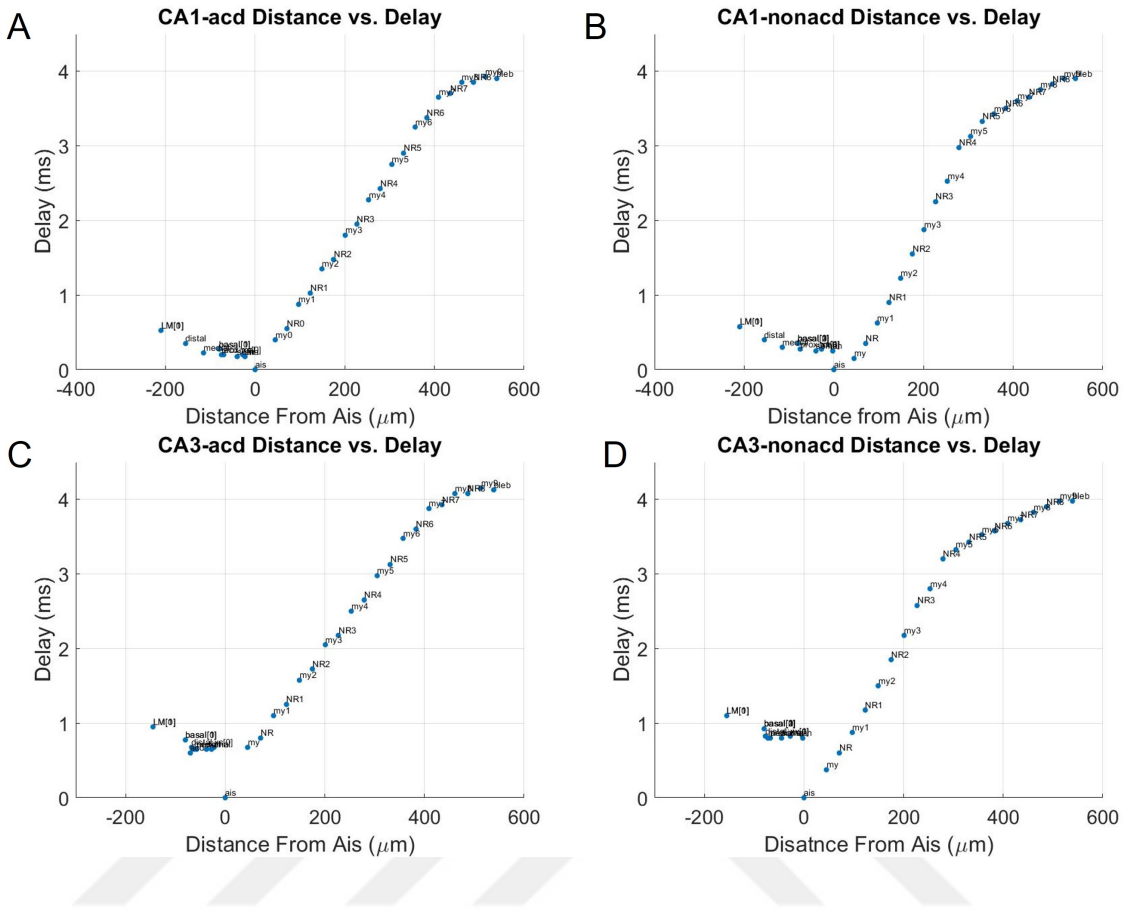

Figure 3.12 Distance from AIS vs. delay of V_{max} of compartments with $I_{0.6}$ injection (A) Distance vs. Delay plot of CA1-AcD cell (B)Distance vs. Delay plot of CA1-nonAcD cell (C)Distance vs. Delay plot of CA3-AcD cell (D)Distance vs. Delay plot of CA3-nonAcD cell.

With $I_{0.6}$ injection, the delays of bleb sections are found to be almost the same when AcD and nonAcD models are compared. However, delay in CA3-AcD cell is slightly more than delay of CA3-nonAcD cell. Delays in basal dendrites are slightly lower in AcD cells compared to nonAcD cells. The trends are again consistent in both AcD cells and nonAcD cells.

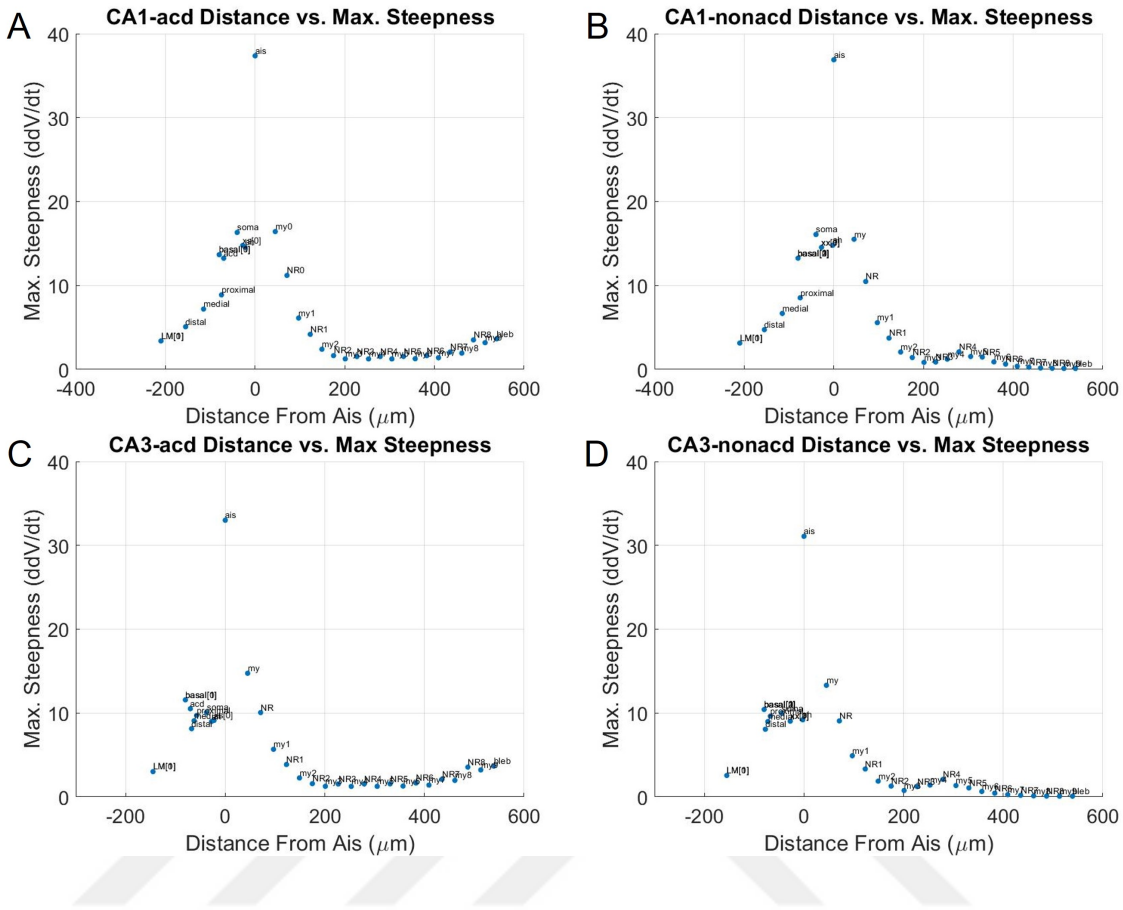

Figure 3.13 $\ddot{V}_{max}$ of each compartment according to their distance from AIS with $I_{0.6}$ injection (A) Distance from AIS vs. $\ddot{V}_{max}$ of CA1-AcD cell. (B)Distance from AIS vs. $\ddot{V}_{max}$ of CA1-nonAcD cell. (C)Distance from AIS vs. $\ddot{V}_{max}$ of CA3-AcD cell. (D)Distance from AIS vs. $\ddot{V}_{max}$ of CA3-nonAcD cell.

The $\ddot{V}_{max}$ trends in AcD cells are found to be different than nonAcD cells. In AcD cells the $\ddot{V}_{max}$ decreases as the potential is propagated through the axon, and then starts increasing at the end of the axon. In nonAcD cells, the $\ddot{V}_{max}$ drops as in AcD, but a small increase in the middle of axon is observed, which is followed by a decrease until the end of the bleb.

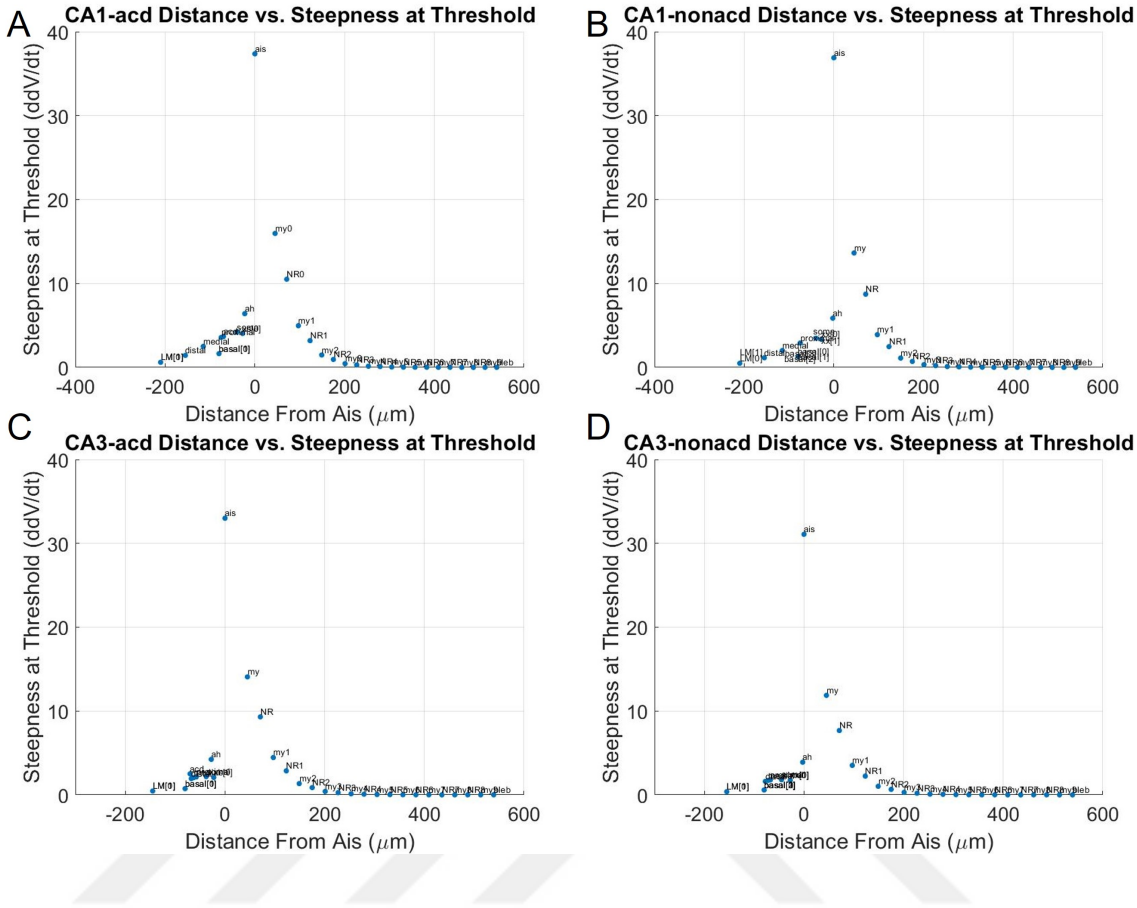

Figure 3.14 Distance from AIS vs. $\ddot{V}_{thr}$ of each compartment at the time $\ddot{V}_{max}$ of AIS is at its maximum with $I_{0.6}$(A)(A) Distance from AIS vs. $\ddot{V}_{thr}$ of CA1-AcD cell. (B)Distance from AIS vs. $\ddot{V}_{thr}$ amplitudes of CA1-nonAcD cell. (C)Distance from AIS vs. $\ddot{V}_{thr}$ amplitudes of CA3-AcD cell. (D)Distance from AIS vs. $\ddot{V}_{thr}$ amplitudes of CA3-nonAcD cell.

The $\ddot{V}_{thr}$ properties of the compartments changed slightly with the increased current injection of $I_{0.6}$. The neighboring cells have slightly steeper potentials in the AcD cells compared to nonAcD cells. With the I_{min} injection, the $\ddot{V}_{thr}$ amplitudes of my0 compartments were almost identical in AcD and nonAcD cells. AcD cells are more responsive to increased current injection compared to nonAcD cells.

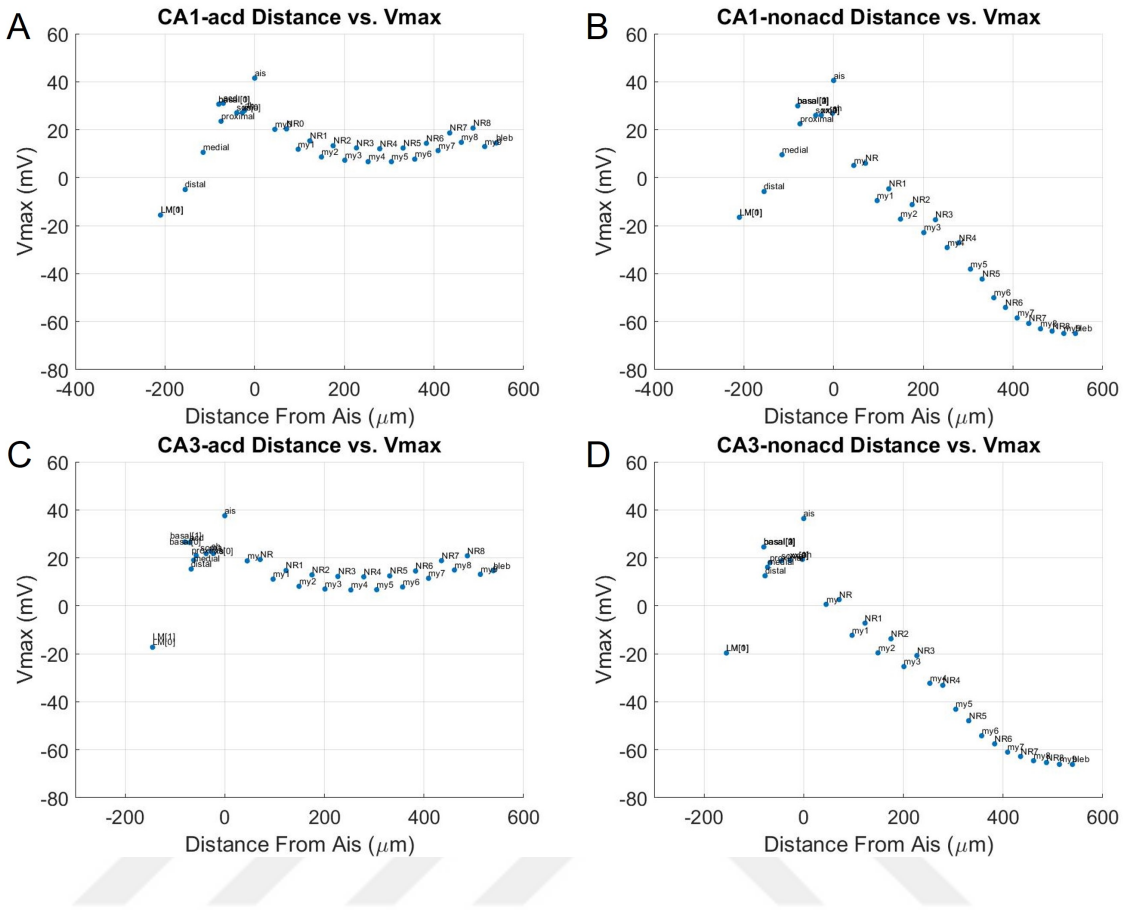

Figure 3.15 Distance from AIS vs. V_{max} of each compartment with $I_{0.6}$ injection (A) Distance from AIS vs. V_{max} of CA1-AcD cell. (B)Distance from AIS vs. V_{max} of CA1-nonAcD cell. (C)Distance from AIS vs. V_{max} of CA3-AcD cell. (D)Distance from AIS vs. V_{max} of CA3-nonAcD cell.

The difference in V_{max} trends in AcD and nonAcD cells did not change with the $I_{0.6}$ injection when compared to the trends with I_{min} injection. However, the potential that is propagated to bleb is higher under $I_{0.6}$ compared to I_{min}.

3.3 Without Basal Dendrites

To understand the effect of topological differences in AcD and nonAcD cells, the basal dendrites are removed from all of the cells. The same experimental procedures are carried on with cells without dendritic trees.

After the current injections are applied, I_{min} is found to be exactly the same (in 4 significant figure precision). As a result, the APs, phase plots, delays, steepness plots and potential plots are found to be exactly the same as the plots shown in the "Minimum Current" section. For this reason, the same plots are not shown here not to cause a repetition.

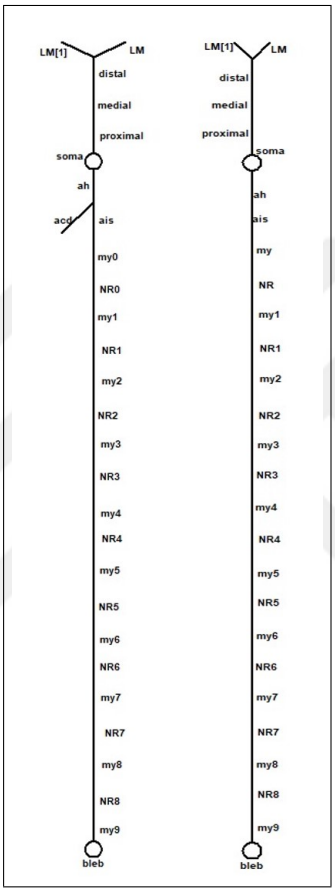

Figure 3.16 Geometries of AcD and nonAcD cells without basal dendrites (A) Branchless geometry of CA1 and CA3 AcD cells (B) Branchless geometry of CA1 and CA3 nonAcD cells.

4. DISCUSSION

The first difference between AcD and nonAcD cells was the I_{min} for AP firing. I_{min} is lower in AcD models compared to the nonAcD models both in CA1 and CA3 cells. This implies that AcD models are more responsive to injected input and more readily to respond compared to nonAcD cells.

Since the biophysical properties of the cells are exactly the same, cell geometry should be the reason for the responsiveness of AcD cells. We know that the dendrites have a significant role in enhancement of the synaptic input. First of all, AcDs are located closer to AIS -where the AP generation is triggered- compared to nonAcDs. In real cells, this helps the distance between the synaptic input zone and the AIS to be lower. However, in the model the I_{min} is injected from soma and diffused to each compartment from there. From the results, we see that the enhancement of the dendrite that is very close to AIS helps the cell to initiate an AP more readily compared to nonAcDs. In nonAcD models, the I_{min} enhancement from basal dendrites has to pass through soma in order to reach the AIS, this reduces its efficacy. Another reason might be its isolation from soma compared to nonAcDs which could result in current loss. The differences between the CA1 cells and the CA3 cells are due to the topological differences as well; diameter of the soma in CA1 cells is 30 μm, whereas it is 40 μm in CA3 cells. For this reason, I_{min} required for CA3 cells is higher than CA1 cells as expected.

The AP waveforms of soma and AIS are similar under I_{min} injection when the AcD and nonAcD cells are compared. This is expected since the same biophysical properties are used in the each model. AcD does not seem to have an effect in the waveforms of the APs.

To analyze further, phase plots are examined. The rate of APs can be observed in more detail with the help of phase plot diagrams. But in the phase plot diagrams

no significant difference is observed as well under I_{min} injection.

When the potential waveforms of each compartment are analyzed, a significant difference between the AcD and nonAcD cells can be observed and this difference is consistent between the AcD and nonAcD cells. The potentials attenuate in nonAcD cells while they are conserved in nonAcD cells. This trend shown with the I_{min} injection does not change with the $I_{0.6}$ injection. Thus we can interpret that the difference in the trends are due to the geometrical differences that is to say the AcD. In order to strengthen this idea, the compartments are analyzed further which resulted in the same conclusion.

Another significant difference between the AcD and nonAcD models is the peak potential the compartments. The figures show that in the nonAcD models the AP is attenuated as the potential is propagated from AIS to axon terminal. In AcD models the potential is conserved and the amplitude is high even in the axon terminal.

Since the difference is so significant, other possible causes are examined. There was a possibility that the nonAcD models could react slower but more steadily and this could be overlooked under I_{min} injection. For this purpose, I_{inj} is increased to a certain amplitude which is higher than the thresholds of each cell yet, low enough to avoid tetanic response.

For this purpose a new I_{inj} is determined. Among the four types, the highest I_{min} belongs to CA3 nonAcD cell, which is 0.5666 nA. 0.6 nA would meet the requirements, so 0.6 nA current is injected to test the possibility. If non-AcD models respond to I_{inj} slower, but conserve it better than AcD cells, we expect to see higher peak potential values in the axon terminal compared to AcD cells under $I_{0.6}$.

However, $I_{0.6}$ did not change the trend in the peak potentials in both CA1 and CA3, AcD and nonAcD cells. Figure 3.21 shows the results of peak potentials of compartments under $I_{0.6}$. These results show that the trends in the peak potential values are independent of the I_{inj} and depend only on the geometries of the cells. The

peak potentials under $I_{0.6}$ are higher than the ones under I_{min} as expected.

Since the biophysical properties are exactly the same, geometrical properties are examined. Even though the topologies are kept as identical and symmetrical as possible, they are not exactly the same. In nonAcD models, there are four basal dendrites connected to soma however, in AcD models there are two basal dendrites connected to soma and one dendrite connected to soma and axon. Another possibility of the sharp difference in the trends of peak potentials between AcD and nonAcD cells was the differences in the number of branches. The current had to flow to more branches in nonAcD cells compared to AcD cells so, the I_{inj} could be insufficient to propagate to axon terminal and attenuate in nonAcD cells.

In order to test this phenomenon, the basal dendrites are eliminated from the models. NonAcD cells had only an axon connected to soma and AcD cells had a dendrite carrying the axon. If higher number of branches cause I_{inj} to spread too much that the axon terminal cannot be fed with the I_{inj} then, with this models we expect to see higher peak potentials in nonAcD models compared to AcD models since the new branchless nonAcD models have less branches than AcD cells.

On the contrary, trends of peak potentials were exactly the same with the models with branches. In this new set-up, AcD cells had more branches than nonAcD cells and they had exactly the same biophysical properties. However, the AcD cells conserved the I_{inj} better than nonAcD cells again, the peak potential is attenuated in the nonAcD cells. These results prove that the difference in conservation and attenuation of I_{inj} is only due to axon being connected to dendrite, it is not due to insufficient I_{inj} or number of dendritic branches.

The experiment is carried on with elimination of basal dendrites showed another aspect. I_{min} was also exactly the same with the cells with basal dendrites (with 5 significant number accuracy). The following characteristics including delay,$\ddot{V}_{max}$ and $\ddot{V}_{thr}$ remained also the same. For this reason the results of the models without branches are not shown in this thesis. Having the same results can be interpreted as basal

dendrites connected to soma are not significant in the propagation of I_{inj}.

AcD is found to be an important feature in I_{min} conservation along the axon. In the basal dendrites and LM compartments the difference is not as significant as the axon terminals, but still V_{max} is slightly higher at these compartments in AcD cells compared to nonAcD cells. When the dendritic branches are compared the AcD has 3 mV higher V_{max} than other basal dendrites in CA1 AcD model. The difference between the V_{max} of AcD and other basal dendrites is 5 mV in CA3 AcD cell. AcD geometry conserves the I_{min} but it also gives a privilege to the dendrite which carries the axon. Thus it may be an important feature for cell to prefer ACD model to nonAcD model.

Another significant difference between the AcD and nonAcD cells was their delay properties. $\triangle t_{peak}$ plots show another aspect of V_{max} propagation; how fast the V_{max} is propagated. Under I_{min} injection, the $\triangle t_{peak}$ in AcD cells is higher than nonAcD cells along the axon. The $\triangle t_{peak}$ in the bleb of CA1 non-AcD cell is 0.775 ms lower than CA1 AcD cell. The difference is 0.875 ms in CA3 cells, $\triangle t_{peak}$ in AcD is higher than nonAcD again.

However, when the other side of the cells are examined, the same plot shows that the $\triangle t_{peak}$ of basal and apical dendrites in AcD cells are lower than nonAcD cells. To be more precise, the $\triangle t_{peak}$ is 0.025 ms lower in basal dendrites of both CA1 and CA3 model cells. In LM compartments of both CA1 AcD and CA3 AcD $\triangle t_{peak}$ is 0.05 ms lower than CA1 nonAcD and CA3 nonAcD models.

The differences between the I_{min} and $I_{0.6}$ injections show another aspect of the cells. With the $I_{0.6}$ injection, the delays of the blebs approached to the delays of blebs under I_{min} injection. On the contrary, delays in basal dendrites and LMs decreased even more under $I_{0.6}$ injection. Under $I_{0.6}$ injection, the delay of the bleb in CA1-AcD and CA1-nonAcD is the same and in CA3-nonAcD it is 0.15 ms lower than CA3-AcD. Delay of the basal dendrites under $I_{0.6}$ injection in CA1-AcD is 0.08 ms lower than CA1-nonacd and in CA3-AcD, it is 0.15 ms lower than CA3-nonAcD. Delay of the LM under $I_{0.6}$ injection in CA1-AcD is 0.05 ms lower than CA1-nonAcD and in CA3-AcD,

it is 0.15 ms lower than CA3-nonAcD.

Delay data clearly shows that AcD models prefer dendrites rather than axon terminal unlike the classical nonAcD cells. This implies that AcD formation may be important neither for data transmission to other cells, nor to increase the processing speed but to process the data more efficiently.

Under $I_{0.6}$ injection, the AP waveforms look almost identical. The shoulder that can be observed at the peak points of the AISs is disappeared due to high current injection. It can only be observed in the CA3 cells since the difference between the I_{min} and $I_{0.6}$ is lower in CA3 cells compared to CA1 cells. This difference can be observed in the phase plot diagrams even in more detail.

$\ddot{V}_{max}$ data shows the maximum steepness of the potential of each compartment. From the $\ddot{V}_{max}$ plot, we can see the responsiveness in the nonAcD cells are lower compared to AcD cells. V_{max} plot showed the amplitude of the propagated potential, but the $\ddot{V}$ is also higher in the AcD cells. Especially at the end of the axon, the $\ddot{V}$ starts increasing again which is a major difference between the nonAcD cells. This trend cannot be explained with the current sufficiency since the same trend can be observed with $I_{0.6}$ injection as well.

$\ddot{V}_{thr}$ data shows the steepness of the potentials of each compartment when the steepness of the AIS is at its maximum. From the plot we can examine the diffusion of the potentials. The $\ddot{V}_{thr}$ values are quite similar in AcD and nonAcD cells when the neighboring compartments are examined such as my0. AcD cells have slightly higher $\ddot{V}_{thr}$ amplitudes compared to nonAcD cells. When the $I_{0.6}$ is injected to the cells. The gap between the $\ddot{V}_{thr}$ of the AcD and nonAcD cells increases. Under $I_{0.6}$ injection, AcD cells have higher $\ddot{V}_{thr}$ values in neighboring compartments compared to nonAcD cells.

To analyze the excitability types of the cells, FI curves are plotted for each cell. All of the cells are found to show Type I properties. The excitabilities of the AcD cells are significantly higher than nonAcD cells. For nonAcD cells to reach to the same

firing rate with the AcD cells, they require an additional 0.5 nA current. The CA1 cells are more excitable than CA3 cells both in AcD and in nonAcD, which can be interpreted as a result of the geometrical differences. CA1-AcD is the first cell to give tetanic response to increasing current injections.

Statistical analysis could not be applied in this research because of the model's properties. Since this is not a real cell the data pool is limited to 1 dataset. This could be improved by adding noise to the input so that every injection gives a different result. However, with the NEURON simulation program this was not possible with graphic user interface.

Because of the novelty of the discovery, the literature on this topic is very limited. The article of Thome et al. suggests a privilege on AcDs compared to nonAcDs. In this study this claim is proven by the V_{max} amplitudes of AcDs and nonAcDs. In CA1-AcD model, the AcD has 3mV higher V_{max} than nonAcD and in CA3-AcD model, the AcD has 5mV higher V_{max}. Also when the delays are examined, in CA1-AcD model, V_{max} is reached 0.075 ms before the nonAcD branch and in CA3-AcD model, V_{max} is reached 0.3 ms before the non-AcD branch. These results are compatible with the experimental data obtained from live cells.

In that article, they have found the EPSP properties and the decay time of the AcDs and nonAcDs are similar from the patch-clamp recordings, they do not show any difference. This is also in line with results of our model. This shows that the conductances that assist the synaptic integration are similar in both AcD and nonAcDs and in our model the biophysical properties are kept the same as in real cells.

Even though the EPSP characteristics are similar, dendritic spines enhance the input cooperativity with synaptic amplification [57]. According to Thome et al., this property of dendritic enhancement is particularly better in AcDs. The V_{max} plot shows this difference quite strikingly. The conservation of V_{max} in AcD cells can be explained with the dendritic enhancement of the AcD while the V_{max} is being attenuated in the nonAcD models.

Another difference the article mentions is the efficacy of synaptic input to generate AP is higher in AcDs compared to nonAcDs. We can prove that with the I_{min} amplitudes in our model. We found that the AcD cells generate APs with lower I_{min} amplitudes compared to nonAcD cells, meaning that the AcD cells use the input more effectively to generate AP and they are more responsive than the nonAcD cells. The difference that can be noted here is the input generation; in this model we did not use synapses to generate AP, the I_{min} is injected from soma.

5. CONCLUSION and FUTURE WORKS

Existence of neurons with AcD is not a new discovery. However, they were considered to be an anomaly and that they won't be observed under normal conditions. Thome et al. showed that this formation is not a malformation; on the contrary, 50% of the CA1 pyramidal neurons and 30% of the CA3 pyramidal neurons have this feature.

The starting point of our study was to discover the purpose of this formation. If certain cells in certain regions have AcD and if they have a fixed distribution even in the same region, then this must bear a purpose.

The biological systems tend to conserve energy as much as possible. When they go under this kind of differentiation, the efficiency and energy should be conserved. The reason for such a dramatic change could be improving signal processing and transmission. However, our findings show that the purpose of this formation might be to use the signal efficiently.

Even though the AcD formation did not quite help the cell with the propagation rate, they are found to conserve the potential along the cell much better than the nonAcD cells. It does not result in a change in the AP waveform. However, the AcD cells are more responsive to current injections.

Keeping in mind that the AcD branches are more privileged than the nonAcD branches, this formation can be helpful if the cells need to keep the information themselves and process that information more than transmitting it. This idea leads us to the term "plasticity".

We know the importance of synaptic plasticity in learning and memory. With the information that the AcD formation is concentrated primarily in hippocampal CA1 and CA3 pyramidal neurons in high percentages, this interpretation is rational. The

main purpose of the AcD may be to give privilege to the dendritic branch which carries the axon rather than axon being connected to the dendrite.

AcD cells in hippocampus are found to be concentrated on precise locations even in their own subregions. We also know that the CA1 pyramidal neurons receive input from CA3 afferents. This may also have a reason; the AcD cells can have distinctive properties when they are in a network. In order to analyze the AcD cell behavior in network, another modeling study is being carried on.

To completely analyze the AcD cell network, the projections to CA1 and CA3 pyramidal cells should be further investigated whether the AcD or nonAcD cells are targeted. This may spot a light on the learning and memory process across the regions.

APPENDIX A. Data Points

A.1 CA1-AcD

Table A.1
Compartments of CA1-acd cell model, their distance from soma, their steepness at threshold, maximum steepness and delay of their maximum potential values.

CA1-AcD	Dist. (μm)	Vmax (mV)	St. at th.(V/s)	Max. st. (V/s)	Delay (ms)
LMs	-210	-29.0378	0.288	1.548	1.375
distal	-155	-18.3727	6.212	2.392	1.200
medial	-115	-4.6447	2.040	3.448	1.125
basal[0]	-80	19.0681	0.628	7.728	1.250
proximal	-75	7.3125	1.552	5.644	1.100
acd	-70	16.8530	1.704	6.744	1.025
soma	-40	10.3702	1.856	10.640	1.075
xs[0]	-27.5	10.5858	1.776	9.628	1.100
ah	-22.5	10.8133	3.128	9.496	1.075
ais	0	30.7155	21.016	21.016	0
my0	45	10.1888	9.212	10.072	0.800
NR0	71	12.7719	6.212	7.156	0.925
my1	97	6.4933	3.108	4.252	1.200
NR1	123	10.8454	2.040	2.952	1.350
my2	149	5.1171	1.000	1.812	1.675
NR2	175	10.4209	0.652	1.396	1.825
my3	201	5.0845	0.328	1.156	2.150
NR3	227	10.7357	0.220	1.452	2.300
my4	253	5.5225	0.108	1.196	2.625
NR4	279	11.2812	0.068	1.492	2.775
my5	305	6.1967	0.036	1.228	3.100
NR5	331	12.1550	0.028	1.544	3.250
my6	357	7.7209	0.012	1.284	3.600
NR6	383	14.5030	0.008	1.668	3.725
my7	409	11.5254	0.004	1.416	4.000
NR7	435	18.9292	0.000	2.120	4.050
my8	461	15.0512	0.000	1.984	4.175
NR8	487	21.0037	0.000	3.592	4.200
my9	513	13.3026	0.000	3.252	4.275
bleb	539	14.8233	0.000	3.716	4.250

A.2 CA1-nonAcD

Table A.2
Compartments of CA1-nonacd cell model, their distance from soma, their steepness at threshold, maximum steepness and delay of their maximum potential values.

CA1-nonAcD	Dist.(μm)	Vmax(mV)	St. at th.(V/s)	Max. st. (V/s)	Delay (ms)
LMs	-210	-29.5024	0.3000	1.396	1.425
distal	-155	-18.9216	0.6920	2.140	1.25
medial	-115	-5.4192	1.1880	3.068	1.175
basals	-80	18.6835	0.6720	7.572	1.275
proximal	-75	6.4358	1.6720	6.080	1.15
soma	-40	9.4534	2.0000	11.456	1.15
xx[0]	-27.5	9.8334	1.9080	10.360	1.15
xx[1]	-27.5	9.8334	1.9080	10.360	1.15
ah	-2.5	9.5524	3.4360	10.540	1.125
ais	0	31.1908	22.0800	22.080	0
my	45	-6.3400	9.2200	9.740	0.35
NR	71	-4.7112	6.1160	6.740	0.65
my1	97	-18.9927	2.9720	3.800	0.975
NR1	123	-14.1058	1.9280	2.596	1.325
my2	149	-26.3405	0.9200	1.520	1.625
NR2	175	-22.6325	0.5880	1.708	2.05
my3	201	-34.1703	0.2800	1.560	2.275
NR3	227	-36.5683	0.1840	1.984	2.6
my4	253	-45.8749	0.0840	1.236	2.7
NR4	279	-50.6160	0.0600	0.912	2.775
my5	305	-56.1930	0.0280	0.548	2.875
NR5	331	-59.2621	0.0240	0.376	2.925
my6	357	-62.3685	0.0080	0.232	3
NR6	383	-64.0937	0.0120	0.160	3.05
my7	409	-65.7934	0.0040	0.100	3.15
NR7	435	-66.6988	0.0000	0.072	3.225
my8	461	-67.5779	0.0000	0.048	3.325
NR8	487	-67.9615	0.0000	0.040	3.375
my9	513	-68.3306	0.0000	0.036	3.475
bleb	539	-68.3424	-0.0040	0.036	3.475

A.3 CA3-AcD

Table A.3
Compartments of CA3-acd cell model, their distance from soma, their steepness at threshold, maximum steepness and delay of their maximum potential values.

CA3-acd	Dist.(μm)	Vmax(mV)	St. at th.(V/s)	Max. st. (V/s)	Delay (ms)
LMs	-155	-27.3134	0.292	1.628	1.75
basals	-80	17.885	0.424	7.432	1.625
acd	-70	12.9558	1.448	5.196	1.325
distal	-77.5	2.59681	1.092	7.168	1.5
medial	-72.5	5.77802	1.176	8.000	1.5
proximal	-67.5	7.46759	1.208	8.556	1.475
soma	-45	8.11756	1.224	8.876	1.475
ah	-22.5	7.76491	2.408	7.928	1.475
xs[0]	-27.5	8.46638	1.172	8.036	1.5
ais	0	28.7215	18.840	18.840	0
my	45	7.12582	8.564	9.120	0.6
NR	71	9.98877	5.848	6.580	0.85
my1	97	4.5077	2.980	3.948	1.275
NR1	123	9.60398	1.968	2.760	1.4
my2	149	4.54243	0.984	1.704	1.725
NR2	175	9.98029	0.640	1.316	1.85
my3	201	4.81735	0.324	1.100	2.2
NR3	227	10.4949	0.212	1.436	2.325
my4	253	5.36034	0.104	1.188	2.675
NR4	279	11.1442	0.072	1.488	2.8
my5	305	6.11561	0.040	1.228	3.15
NR5	331	12.0896	0.020	1.544	3.275
my6	357	7.68494	0.016	1.276	3.625
NR6	383	14.4679	0.008	1.668	3.775
my7	409	11.5076	0.004	1.420	4.025
NR7	435	18.9166	0.004	2.120	4.075
my8	461	15.0446	0.004	1.984	4.225
NR8	487	21.0016	0.000	3.592	4.225
my9	513	13.2927	0.004	3.248	4.3
bleb	539	14.8221	0.000	3.716	4.275

A.4 CA3-nonAcD

Table A.4
Compartments of CA3-nonacd cell model, their distance from soma, their steepness at threshold, maximum steepness and delay of their maximum potential values.

CA3-nonAcD	Dist.(μm)	Vmax(mV)	St. at th.(V/s)	Max. st. (V/s)	Delay (ms)
LMs	-155	-27.78	0.284	1.496	1.775
basals	80	17.4378	0.420	7.304	1.65
distal	-77.5	1.90821	1.116	7.616	1.525
medial	-72.5	5.0433	1.200	8.484	1.525
proximal	-67.5	6.71617	1.236	9.092	1.5
soma	-45	7.35862	1.256	9.420	1.5
xx[0]	-27.5	7.83214	1.200	8.528	1.525
xx[1]	-27.5	7.83214	1.200	8.528	1.525
ah	-22.5	6.80209	2.628	8.680	1.5
ais	0	29.9134	20.488	20.488	0
my	45	-7.56238	8.248	9.224	0.325
NR	71	-6.11285	5.452	6.352	0.625
my1	97	-20.4778	2.628	3.624	0.975
NR1	123	-15.5921	1.700	2.472	1.35
my2	149	-27.605	0.812	1.456	1.65
NR2	175	-24.5461	0.532	2.036	2.1
my3	201	-35.9412	0.256	1.632	2.275
NR3	227	-39.3743	0.160	1.780	2.55
my4	253	-48.0143	0.084	1.088	2.625
NR4	279	-52.5284	0.052	0.780	2.7
my5	305	-57.5662	0.024	0.472	2.8
NR5	331	-60.3554	0.012	0.328	2.85
my6	357	-63.1584	0.004	0.200	2.95
NR6	383	-64.7175	0.000	0.140	3
my7	409	-66.252	0.004	0.088	3.075
NR7	435	-67.0695	-0.004	0.064	3.15
my8	461	-67.8637	0.004	0.044	3.25
NR8	487	-68.2108	-0.004	0.036	3.3
my9	513	-68.5442	0.000	0.032	3.4
bleb	539	-68.5555	-0.004	0.032	3.4

REFERENCES

1. Ed S. Lein Bryan A. Strange, Menno P. Witter and Edvard I. Moser. Functional organization of the hippocampal longitudinal axis. *Nature Reviews Neuroscience*, 15(10):655–669, October 2014.

2. N. L. M. Cappaer N. M. van Strien and M. P. Witter. The anatomy of memory: an interactive overview of the parahippocampal-hippocampal network. *Nature Reviews Neuroscience*, 10:272–282, 2009.

3. Philippe Taupin. *The Hippocampus - Neurotransmission and Plasticity in the Nervous System*. Nova Biomedical Books, New York, 2007.

4. Nelson Spruston. Pyramidal neurons: Dendritic structure and synaptic integration. *Nature Reviews Neuroscience*, February 2008. Published online.

5. Saybasili H. Oz P. In vitro detection of oxygen and glucose deprivation-induced neurodegeneration and pharmacological neuroprotection based on hippocampal stratum pyramidale width. *Neuroscience Letters*, (636):196–204, 2017.

6. Greg Stuart Bert Sakmann Nelson Spruston, Yitzhak Schiller. Activity-dependent action potential invasion and calcium influx into hippocampal ca1 dendrites. *Science*, 268(5208):297–300, April 1995.

7. Antonio Yanez Christian Schultz Maren Engelhardt Sidney B. Cambridge Martin Both Andreas Draguhn Heinz Beck Christian Thome, Tony Kelly and Alexei V. Egorov. Axon-carrying dendrites convey privileged synaptic input in hippocampal neurons. *Neuron*, 83(26):1418–1430, September 2014.

8. Wulfram Gerstner and Werner M. Kistler. *Spiking Neuron Models: Single Neurons, Populations, Plasticity*. Cambridge University Press, 2002.

9. Anthony Wright. *Limbic System: Hippocampus*. Department of Neurobiology and Anatomy, The UT Medical School at Houston. Open-access electronic textbook.

10. James J. Knierim. The hippocampus. *Current Biology*, 25:1107–1125, December 2015.

11. O'Keefe J. Nadel L. *The Hippocampus as a Cognitive Map*. Oxford University Press, 1978.

12. Gage FH BuzsÃ¡ki G, Chen LS. Spatial organization of physiological activity in the hippocampal region: relevance to memory formation. *Progress in Brain Research*, 83:257–268, 1990.

13. RE; Broadbent NJ; Squire LR Clark. Hippocampus and remote spatial memory in rats. *Hippocampus*, 15(2):260–272, 2005.

14. F; Morales D; Montiel J Aboitiz. The evolutionary origin of the mammalian isocortex: Towards an integrated developmental and functional approach. *Behavioral and Brain Sciences*, 26(5):535–552, 2003.

15. Matthew W. Jones and Thomas J. McHugh. Updating hippocampal representations: Ca2 joins the circuit. *Trends in Neuroscience*, 34(10):526–535, October 2011.

16. R Lorente de No. Studies on the structure of the cerebral cortex. ii. continuation of the study of the ammonic system. *Journal of Neurology and Psychology*, 46:113–177, 1934.

17. Leutgeb J.K. Treves A. Moser M.B. Leutgeb, S. and E.I. Moser. Distinct ensemble codes in hippocampal areas ca3 and ca1. *Science*, 305:1295–1298, 2004.

18. Yoganarasimha D. Rao G. Lee, I. and J.J. Knierim. Comparison of population coherence of place cells in hippocampal subfields ca1 and ca3. *Nature*, 430:456–459, July 2004.

19. Bliss T.V. Lomo T. Olsen L.I. Andersen, P. and K.K. Skrede. Lamellar organization of hippocampal excitatory pathways. *Acta Physiologica Scandinavica*, 76:4A–5A, 1969.

20. Moser EI Moser MB. Igarashi KM2, Ito HT. Functional diversity along the transverse axis of hippocampal area ca1. *FBBS Letters*, 588(15):2470–2476, August 2014.

21. Quinn JJ Balthasar N Coppari R Elmquist JK Lowell BB Fanselow MS Wilson MA Tonegawa S. McHugh TJ, Jones MW. Dentate gyrus nmda receptors mediate rapid pattern separation in the hippocampal network. *Science*, 317(5834):94–99, July 2007.

22. Gyorgy Buzsaki. Feed-forward inhibition in the hippocampal formation. *Progress in Neurobiology*, 22:131–153, December 1984.

23. S. Ramon y Cajal. *Histology of the Nervous System of Man and Vertebrates*. Oxford Univ. Press, Oxford, 1995.

24. Panzica F Radici C Avanzini G. Franceschetti S, Sancini G. Postnatal differentiation of firing properties and morphological characteristics in layer v pyramidal neurons of the sensorimotor cortex. *Neuroscience*, 83(4):1013–1024, April 1998.

25. DG Amaral N. Ishizuka, J. Weber. Organization of intrahippocampal projections originating from ca3 pyramidal cells in the rat. *Journal of Comparative Neurology*, 295(4):580–623, May 1990.

26. Guy N. Elston. Cortex, cognition and the cell: New insights into the pyramidal neuron and prefrontal function. *Cerebral Cortex*, 13(11):1124–1138, November 2003.

27. Freund TF Gulyas AI Megias M, Emri Z. Total number and distribution of inhibitory and excitatory synapses on hippocampal ca1 pyramidal cells. *Neuroscience*, 102(3):527–540, 2001.

28. Susumu Tonegawa Joe Z Tsien, Patricio T Huerta. The essential role of hippocampal ca1 nmda receptor dependent synaptic plasticity in spatial memory. *Cell*, 87(7):1327–1338, December 1996.

29. Otmakhova NA. Lisman JE. Storage, recall, and novelty detection of sequences by the hippocampus elaborating on the socratic model to account for normal and aberrant effects of dopamine. *Hippocampus*, 11(5):551–568, 2001.

30. Maguire EA. Kumaran D. Which computational mechanisms operate in the hippocampus during novelty detection. *Hippocampus*, 17(9):735–748, 2007.

31. Thomas J. McHugh Derek L. Buhl Susumu Tonegawa Toshiaki Nakashiba, Jennie Z. Young. Transgenic inhibition of synaptic transmission reveals role of ca3 output in hippocampal learning. *Science*, 319(5867):1260–1264, February 2008.

32. Amaral DG. Ishizuka N, Weber J. Organization of intrahippocampal projections originating from ca3 pyramidal cells in the rat. *Journal of Comperative Neurology*, 295(4):580–623, May 1990.

33. Matsuki N Ikegaya Y. Sasaki T, Takahashi N. Fast and accurate detection of action potentials from somatic calcium fluctuations. *Journal of Neurophysiology*, 100(3):1668–1676, September 2008.

34. Malinow R. Liao D, Hessler NA. Activation of postsynaptically silent synapses during pairing-induced ltp in ca1 region of hippocampal slice. *Nature*, 375(6530):400–404, June 1995.

35. Quirk MC Rondi-Reig L Wilson MA Tonegawa S Nakazawa K, Sun LD. Hippocampal ca3 nmda receptors are crucial for memory acquisition of one-time experience. *Neuron*, 38(2):305–315, April 2003.

36. F. J. Brinley JR. E. R. Kandel, W. A. Spencer. Electrophysiology of hippocampal neurons: I. sequential invasion and synaptic organization. *Journal of Neurophysiology*, 24(3):225–243, September 1960.

37. Eccles JC. *The physiology of synapses.* New York: Academic, New York, 1964.

38. Stephen R. Williams and Greg J. Stuart. Dependence of epsp efficacy on synapse location in neocortical pyramidal neurons. *Science*, 295:1907–1910, March 2002.

39. Yael Katz William L. Kath Nelson Spruston Nace L. Golding, Timothy J. Mickus. Factors mediating powerful voltage attenuation along ca1 pyramidal neuron dendrites. *The Journal of Phsiology*, 568(1):69–82, October 2005.

40. Stephen R. Williams and Greg J. Stuart. Role of dendritic synapse location in the control of action potential output. *Trends in Neuroscience*, 26(3):147–154, March 2003.

41. Jarsky T. Martina M. Spruston N. Metz, A. E. R-type calcium channels contribute to afterdepolarization and bursting in hippocampal ca1 pyramidal neurons. *Journal of Neuroscience*, 25:5763–5773, 2005.

42. Proskauer C.C. Peters, A. and I.R. Kaiserman-Abramof. The small pyramidal neuron of the rat cerebral cortex. the axon hillock and initial segment. *Journal of Cell Biology*, 39:604–619, 1968.

43. J.J. Sloper and T.P. Powell. A study of the axon initial segment and proximal axon of neurons in the primate motor and somatic sensory cortices. *Philosophical Transactions of the Royal Society of London. Series B, Biological Sciences*, 285:173–197, 1979.

44. Iremonger K.J. Constantin S. Herde, M.K. and A.E. Herbison. Gnrh neurons elaborate a long-range projection with shared axonal and dendritic functions. *Journal of Neuroscience*, 33:12689–12697, July 2013.

45. Stuart G. Racca C. Hausser, M. and B. Sakmann. Axonal initiation and active dendritic propagation of action potentials in substantia nigra neurons. *Neuron*, 15:637–647, 1995.

46. Vida I. Martina, M. and P. Jonas. Distal initiation and active propagation of action potentials in interneuron dendrites. *Science*, 287:295–300, 2000.

47. Alon Polsky Gal Ariav and Jackie Schiller. Submillisecond precision of the input-output transformation function mediated by fast sodium dendritic spikes in basal dendrites of ca1 pyramidal neurons. *Journal of Neuroscience*, 23(21):7750–7758, August 2003.

48. Branco T Hausser M.r Smith SL, Smith IT. Dendritic spikes enhance stimulus selectivity in cortical neurons in vivo. *Nature*, 503(7474):115–120, November 2013.

49. Wilfrid Rall. Branching dendritic trees and motoneuron membrane resistivity. *Experimental Neurology*, 1(5):495–527, 1959.

50. Wilfrid Rall. *Cable Theory for Dendritic Neurons*. MIT Press, 1989.

51. A. L. Hodgkin and A. F. Huxley. A quantitative description of membrane current and its application to conduction and excitation in nerve. *The Journal of Physiology*, 117(4):500–544, August 1952.

52. Michael L. Hines Nicholas T. Carnevale. *The NEURON Book*. Cambridge University Press, New Haven, Connecticut, 2004.

53. Michael Rudolph. The neuron simulation environment: A brief introduction. Congress course, International Brain Research Organization, Obidos, Portugal, 2004.

54. Richard Goering. Matlab edges closer to electronic design automation world. *EE Times*, April 2004.

55. Fahri E. Abbott, L. F. and S. Gutmann. The path integral for dendritic trees. *The Journal of Physiology*, 66(1):49–60, May 1991.

56. Masato Okada Masashi Inoue Hiroyoshi Miyakawa Hiromu Monai, Toshiaki Omori and Toru Aonishi. An analytic solution of the cable equation predicts frequency preference of a passive shunt-end cylindrical cable in response to extracellular oscillating electric fields. *Biophysics Journal*, 98(4):524–533, February 2010.

57. Spruston N Kath WL Magee JC. Harnett MT, Makara JK. Synaptic amplification by dendritic spines enhances input cooperativity. *Nature*, 491(7425):599–602, 2012.